ESD-TR-76-321

Project Report

LRP-4

Wideband 10.6 μm Backscatter Range

Interim Report

L. R. Tomasetta
G. M. Carter
M. S. Edelstein

2 November 1976

Prepared for the Defense Advanced Research Projects Agency
under Electronic Systems Division Contract F19628-76-C-0002 by

Lincoln Laboratory
MASSACHUSETTS INSTITUTE OF TECHNOLOGY
LEXINGTON, MASSACHUSETTS

The work reported in this document was performed at Lincoln Laboratory, a center for research operated by Massachusetts Institute of Technology. This work was sponsored by the Defense Advanced Research Projects Agency under Air Force Contract F19628-76-C-0002 (ARPA Order 600).

This report may be reproduced to satisfy needs of U.S. Government agencies.

This technical report has been reviewed and is approved for publication.

FOR THE COMMANDER

Raymond L. Loiselle

Raymond L. Loiselle, Lt. Col., USAF
Chief, ESD Lincoln Laboratory Project Office

MASSACHUSETTS INSTITUTE OF TECHNOLOGY

LINCOLN LABORATORY

WIDEBAND 10.6 μm BACKSCATTER RANGE

INTERIM REPORT

L. R. TOMASETTA
G. M. CARTER
Group 54

M. S. EDELSTEIN
Group 37

PROJECT REPORT LRP-4

2 NOVEMBER 1976

LEXINGTON MASSACHUSETTS

ABSTRACT

This report summarizes the principles, hardware and performance of a high resolution 10.6 μm optical backscatter range. Included is a description of the backscatter range, optical setup and processing capabilities. Results include demonstration of the high resolution range and doppler capabilities of the wideband waveform as well as the first high resolution 10.6 μm range-resolved angle-angle scanned and range-doppler images.

CONTENTS

LIST OF ILLUSTRATIONS

I. INTRODUCTION

This report summarizes the principles, hardware and performance of a high resolution 10.6 μm optical backscatter range. Included is a description of the backscatter range, optical setup and processing capabilities. Results include demonstration of the high resolution range and doppler capabilities of the wideband waveform as well as the first high resolution 10.6 μm range-resolved angle-angle scanned and range-doppler images. The 10.6 μm backscatter range has operated on a 60 m static range in a wideband mode for over a year and a compilation of the hardware, processing and performance is relevant not only because the results themselves demonstrate the first wideband imaging at 10.6 μm but also because the techniques are applicable to wideband long range infrared radars.

II. SYSTEM OVERVIEW AND HARDWARE

A. Principles of Operation of Optical Chirp Radar

In a radar system targets can be resolved in range by a large number of signal waveforms and processing techniques. Most of the techniques fall into two classes[1]: 1) single frequency pulse techniques where the range resolution is proportional to the inverse of the pulse duration and, 2) multiple frequency or FM chirp techniques where the range resolution is determined by the signal waveform characteristics (i.e., bandwidth, shape, etc.). Although both techniques have been extensively employed in radar systems, the longer duration chirp waveform offers the following advantages over an uncoded pulse of equivalent bandwidth: 1) lower peak power for the same energy per pulse which results in either less expensive components for

equivalent energy systems or greater energy and, therefore, sensitivity for equivalent peak power systems, 2) the ability to doppler process the return is facilitated by the longer duration chirp pulse and the resultant greater time between samples.

The 10.6 μm backscatter range utilizes a microwave waveform generator built by D. Bromagim of Lincoln Laboratory. The details of how the microwave waveform is converted to a 10.6 μm carrier will be discussed in a later section. The waveform is a 1000 MHz linear chirp with a duration of 250 μsec. Figure 1a shows the waveform. Range resolution is accomplished in the following manner. The generated optical waveform is split into two components: the local oscillator (LO) and the signal. The signal portion is used as the radar transmit waveform. The return signal is then optically mixed with the LO. The received signal and LO are identical (neglecting doppler effects) with the exception that the received signal is delayed relative to the LO by the transit time to and from the target (Figure 1b). The result of the optical mixing between a linear frequency ramp and its delayed replica (correlation detection) is a single frequency pulse for the duration of the signal overlap (Figure 1c). The frequency of the pulse is proportional to the range of the target.

For a linear FM chirp radar, let

B = bandwidth of chirp

T = chirp duration

f = correlation detector frequency

τ = transit time of signal path

R = range to target

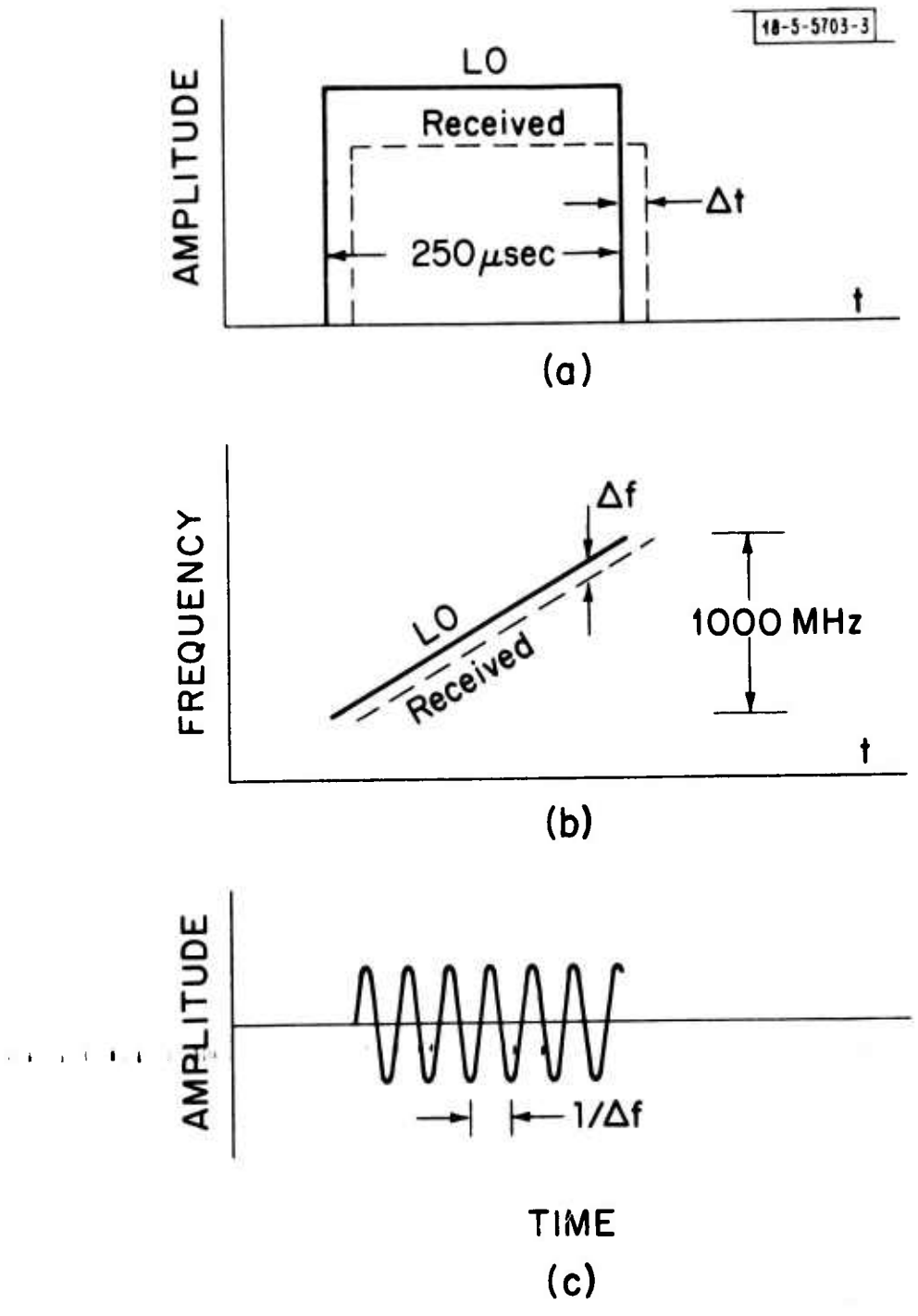

Fig. 1. Wideband waveform and optical correlation technique.

realizing that B/T is the slope of the waveform, df/dt, the correlation frequency is easily seen to be:

$$f = \frac{B}{T}\tau = \frac{B}{T}\frac{2R}{c}$$

for $B = 1000$ MHz

$T = 250$ μsec

$R = 60$ m

then $f = 1.6$ MHz

The range resolution can be derived by realizing that the Fourier Transform of a single frequency pulse is a sinc x function centered at the return frequency with a half power width of 1/T, where T is the pulse duration. The range resolution is therefore

$$\Delta f_{res} = 1/T = 4 \text{ kHz}$$

$$\Delta R_{res} = \frac{T}{2B} c \quad f_{res} = \frac{c}{2B} = 15 \text{ cm}$$

The range resolution indicates the radar's capability to discriminate two point targets of equal cross section separated in range by 15 cm. The importance of performing the correlation at the optical frequency is as follows. Range resolution inherent in a 1000 MHz waveform can be obtained with an optical detector requiring only a few megahertz frequency response. Even if the range of the target is substantially increased so that the delay time is comparable to or even greater than the chirp itself, detector bandwidths can be kept significantly smaller than 1000 MHz by varying the chirp

repetition rate so that the target return from chirp n will mix with LO chirp n + 1. Present 10.6 μm oscillators possess the coherence time required to allow staggered chirp operation.

Crossrange information of a target can be obtained by a number of techniques. We have used two techniques to generate the crossrange information. The first technique (angle-angle) employs a beam much smaller than the target, a raster scanning optical system, and a stationary target. The crossrange information is obtained by correlating the angle-angle position of the scanning system with the appropriate crossrange dimension. The second technique employs the use of target doppler to determine crossrange. In the chirp radar system doppler is measured from pulse-to-pulse phase differences. This requires that the starting phase of the chirp in the signal and LO path have the same phase relation for every chirp and that the laser and other CW microwave carriers be coherent for the transit time. In the backscatter range the signal and LO are generated as a single optical beam and subsequently split so these phase relationships are always maintained. Figure 2 demonstrates how the correlation detector output is affected by a moving target. Figure 2a shows a single stationary target. Figure 2b shows a single moving target. Notice that it is the pulse-to-pulse phase difference that determines the doppler.

For a pulse train of length T_D made up of chirps of duration T, with a 50% duty cycle and a system coherence time greater than T_D the unambiguous doppler excursion is

$$f_{D_{unambiguous}} = \frac{1}{2T} = 2 \text{ kHz}$$

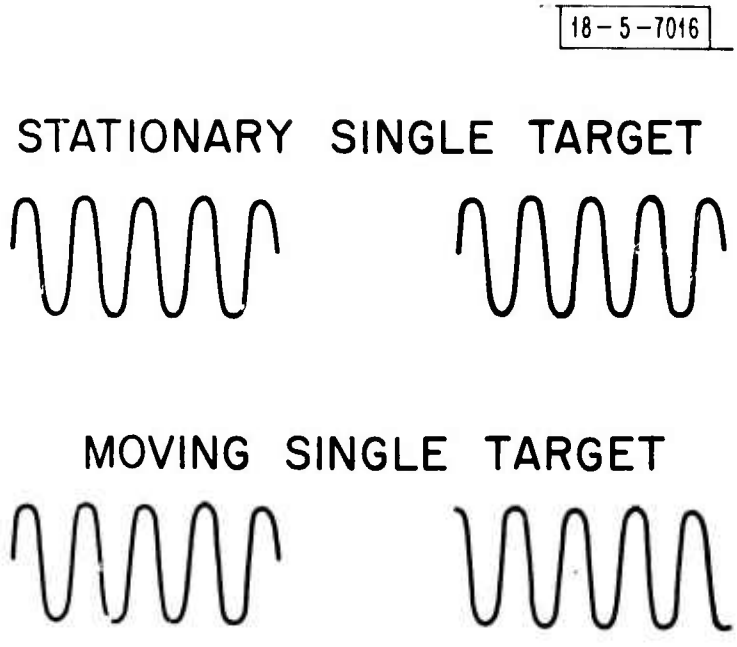

Fig. 2. Chirped radar doppler detection techniques.

The doppler resolution is $f_{D_{unambiguous}} = 1/T_D$. The crossrange position, Δx about the center of a rotation of the fully illuminated target rotating at angularly frequency, ω_r, can be related to measured doppler frequency, f_D, by

$$\Delta x = \frac{\lambda f_D}{2\omega_r}$$

where λ is the optical carrier wavelength. Details of the data processing involved in converting a series of chirps into a range-doppler image will be discussed in a later section.

Two techniques of range-crossrange imaging are used depending on how the crossrange information is derived. 1) Range-resolved angle scanned imaging requires a stationary target and a beamwidth much smaller than the target. For each stationary aspect angle range information will be obtained from the frequency information of the chirp and crossrange information from the angle-angle position of the moveable mirror. To reconstruct an image of the target the range-crossrange images of many aspect angles are superimposed. Figure 3 shows a schematic of this reconstruction technique. 2) Range-doppler imaging requires a slowly rotating target illuminated by a beam comparable to the target size. Information to construct a range-crossrange image can be obtained in a time determined only by the required doppler resolution but in any case before the target rotates more than a fraction of a degree. Range information is obtained from the chirp frequency and crossrange information is now obtained from the doppler frequency distribution. The complete image is again reconstructed by superimposing the images from a large number of aspect angles.

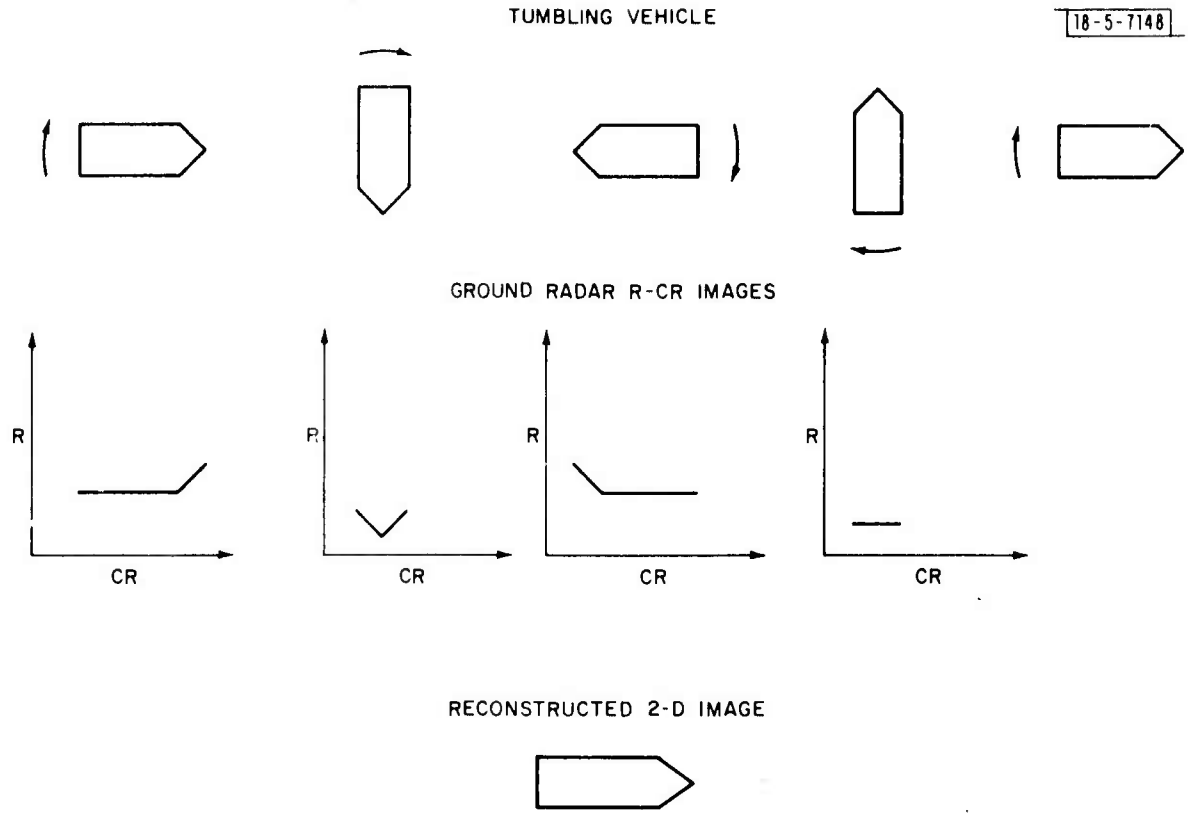

Fig. 3. Range-crossrange imaging.

B. Wideband Infrared Modulator

The infrared modulator was built to produce a wideband infrared sideband (near 10.6 μm) by mixing a CW infrared laser (single mode) output with a chirped microwave signal. The mixing medium is single-crystal GaAs which is transparent in the infrared (~1-16 μm). Applying an electric field (in our case the microwave electric field) to the crystal causes the GaAs to become birefringent for infrared radiation. The single crystal is oriented so that the birefringence produces an elliptically polarized infrared output from a linearly polarized input. This birefringence is modulated at the frequency of the applied electric field and produces sidebands of the infrared carrier frequency, ω_o. By following the modulator with a polarizer oriented 90^o to the input infrared polarization, only the odd sideband frequencies, $\omega_o \pm \omega_m$, $\omega_o \pm 3\omega_m$, etc. (ω_m = microwave frequency) remain. Ideally there is no carrier present and most of the power is in the first sideband ($\omega_o \pm \omega_m$). Residual carrier does leak through the second polarizer because strain, impurity and thermal induced birefringence exist in the crystal.

The modulated birefringence for any infrared phase front is a local phenomena. To produce a net elliptical polarization at the end of the crystal the applied electrical field must be uniform along the length of the crystal. At microwave frequencies this is impossible for a structure longer than $\lambda_m/2$ (λ_m = microwave wavelength). If, however, the applied electric field travels at the same phase velocity through the crystal as the infrared, then the infrared field sees the same microwave field as it

travels through the crystal. This produces a net birefringence modulated at the microwave frequency.

The modulator design used in the backscatter system consists of a 12 cm bar of GaAs placed inside a waveguide cavity. A 6 cm version of the device is shown in Figure 4. The optical field enters through the cuts in the waveguide. The phase velocity of the microwave field can be adjusted by means of moveable shorting plates placed in the cavity. The top of the guide rests on the top of the crystal and is made flexible for good guide-crystal contact. The microwave frequency over which the device can be used is determined by the microwave transmission characteristics of the guide and phase match between the optical and microwave fields.

For either sideband ($\omega_o + \omega_m$ or $\omega_o - \omega_m$) the theoretical maximum sideband output power, P_S, for the scheme described above is

$$P_S = P_o \left(\frac{\pi}{2} \frac{n_o^3 r_{41}}{\lambda_o} E_m L \right)^2$$

where P_o = input infrared carrier power

λ_o = input infrared carrier wavelength in vacuum

n_o = GaAs index of refraction at λ_o (3.27)

r_{41} = electro-optic coefficient of GaAs (1.7×10^{-10} cm/v)

E_m = peak microwave electric field

P_m = average microwave power

L = length of crystal

This approximation is valid for $P_S/P_o < .1$ and neglects optical and microwave losses in the crystal and microwave structure.

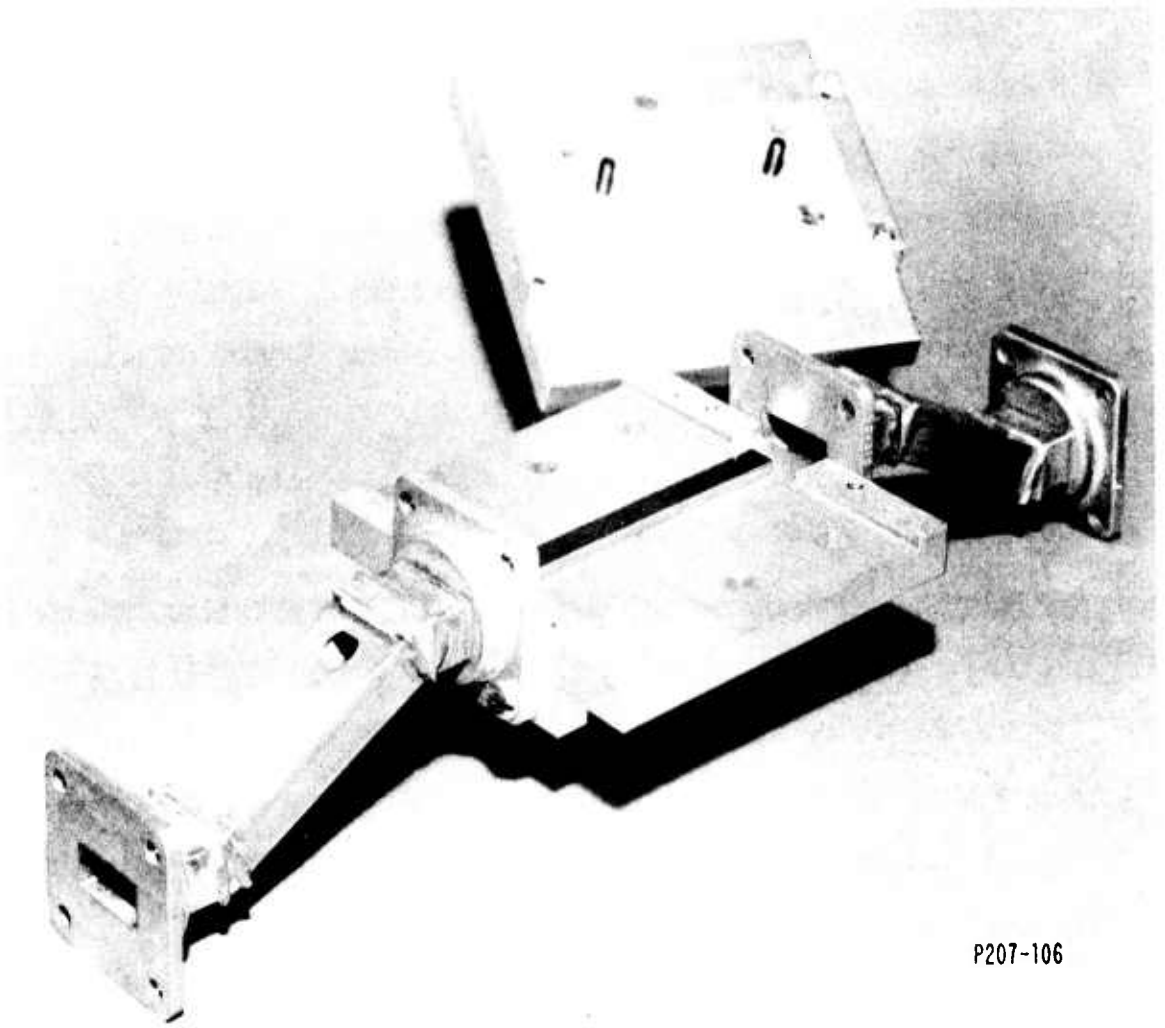

Fig. 4. Wideband infrared modulator.

Thus with P_m = 80 W ($E_m \approx 5 \times 10^2$ V/cm), L = 12 cm, and P_o = 50 W, we calculate $P_S \approx 150$ mW for the lossless case and measure $P_S \approx 30$ mW at f_m = 15.6 GHz. We attribute the difference to: optical losses in the crystal and microwave losses in the crystal and modulator structure.

The phase match bandwidth is greater than 1 GHz. Inductive irises are used to impedance match a 1 GHz flat microwave transmission at 15.6 GHz center frequency.

Table I summarizes the operating parameters and other details of the modulator.

To significantly increase the sideband power output from the modulator would be very expensive if obtained by increased microwave and/or laser power. A more attractive alternative, replacing the GaAs crystals with CdTe, has been chosen to increase the sideband power. CdTe offers two advantages over GaAs, 1) at 10.6 μm CdTe is 4 times as efficient per unit length as GaAs in producing sidebands, 2) the optical losses for CdTe are .2% cm^{-1} compared to 3% cm^{-1} for GaAs. For our given length of crystal (12 cm) the combination of advantages should give us an increase of from 4 to 8 times the optical sideband output. The variability in the improvement exists because the sideband conversion increases as the square of the length of the crystal while the optical and microwave losses which are not precisely known decrease the output exponentially with length.

Until recently, bulk single crystal CdTe has not been available commercially. II-VI Corporation now produces bulk single crystals of CdTe. To increase our sideband power we have purchased single crystal CdTe and have characterized its microwave and optical properties. The next step will be to

TABLE I

MATERIAL PROPERTIES

Material:	GaAs (Cr doped) single crystal oriented for amplitude modulation.
Resistivity:	$\geq 10^6$ ohm-cm
Optical Loss (estimated):	.02 cm^{-1}
Microwave Loss:	.02 cm^{-1}
Length:	12 cm
Width:	.559 cm
Height:	.254 cm

Ar coated ends, polished (.3 μ grit) on top and bottom

Supplier: Coherent Radiation

MODULATOR CHARACTERISTICS

Mechanical Structure:	Traveling wave, reduced height waveguide; flexible top, moveable sides.
Length of GaAs Crystal(s):	12 cm, two crystals as per crystal specs.
Microwave Mode Used:	TE_{10}
Total Optical Loss	≈ 3 dB
Total Microwave Loss:	≈ 3 dB
Microwave Transmission Frequency Range:	≈15-16.5 GHz (3 dB points)
Power Sideband Output:	≈30 mW, 50 W optical (CW) input, 80 watts (CW) microwave input.

obtain a phase match for the microwave and 10.6 μm waves in the CdTe crystal with a test modulator. Then an optimized waveguide structure will be put in the system. The test modulator has been built and a 6 cm CdTe modulator is currently being tested.

C. System Hardware

The system hardware is designed to operate as a coherent 10.6 μm chirped radar. A block diagram of the hardware is shown in Figure 5.

The system hardware can be divided into two functional groups. 1) Equipment to produce the infrared correlated output signal. 2) Data recording and processing equipment.

The radar signal system requires a radar output, a local oscillator, a radar return, and a correlation infrared detector.

The unique part of this radar is the wideband chirped waveform on a 10.6 μm carrier. The 1 GHz chirp is superimposed on the CW laser output by mixing the laser with the microwave chirp in the modulator. The microwave chirp is centered on a 15.6 GHz carrier. The waveform is shown in Figure 1a. This produces an output offset from the laser by 15.6 ± .5 GHz. This particular microwave carrier is used so that in the future, the output can be amplified by an optical amplifier. The oscillator will be a $^{13}C^{18}O_2$ (isotope) laser operating on the R(20) line (near 10.6 μm) and the optical amplifier using ordinary ($^{12}C^{16}O_2$) CO_2 will have a high power line (P(22)) 15.6 GHz away and will thus amplify the upper sideband output of the modulator.

The microwave ramp generator shown in Figure 6 provides the pulse shape that is impressed on the infrared carrier. The pulse width is 250 μsec. The linear excursion of 1 GHz is provided by a VCO with a 6 GHz carrier. The

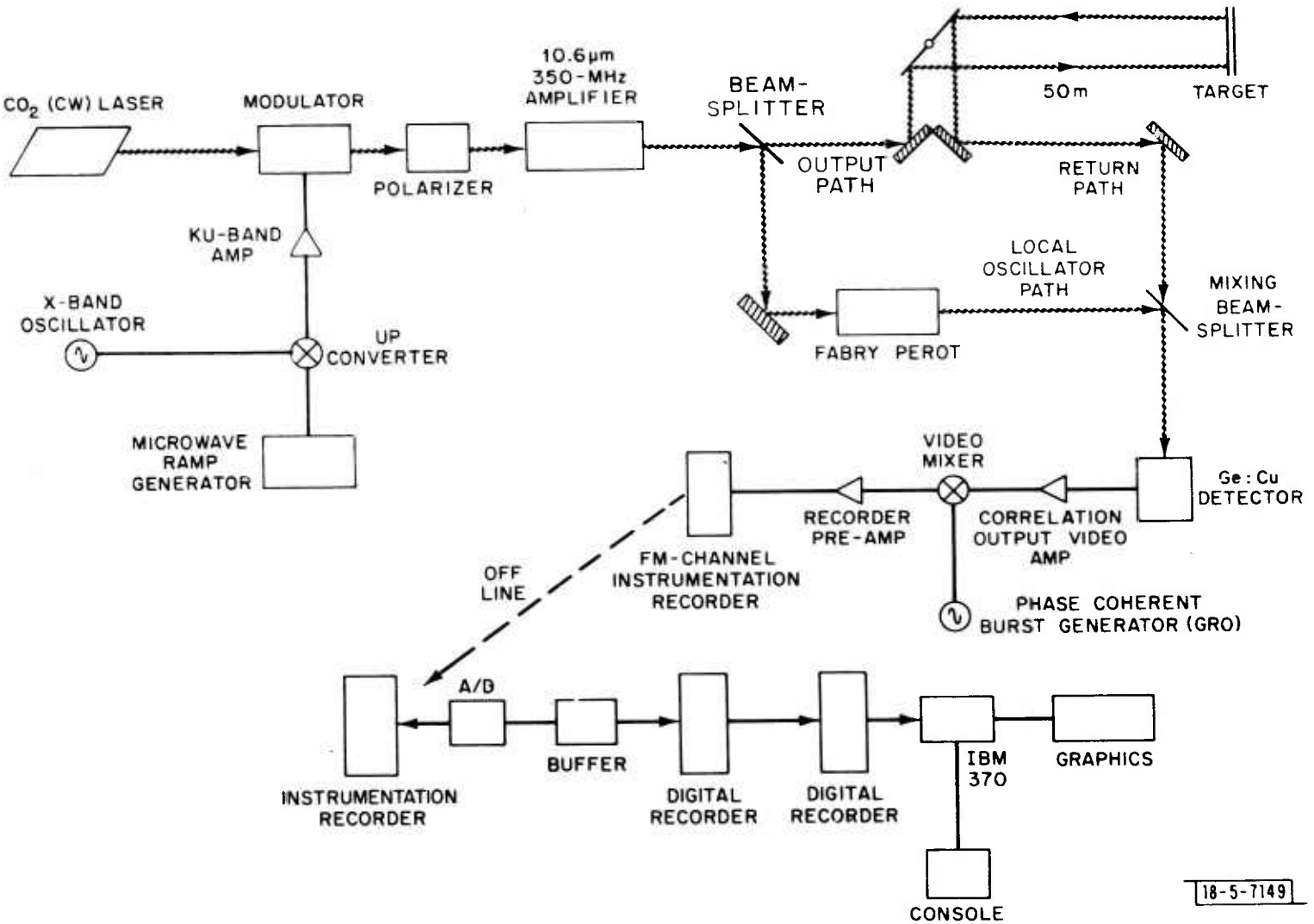

Fig. 5. Optical backscatter hardware.

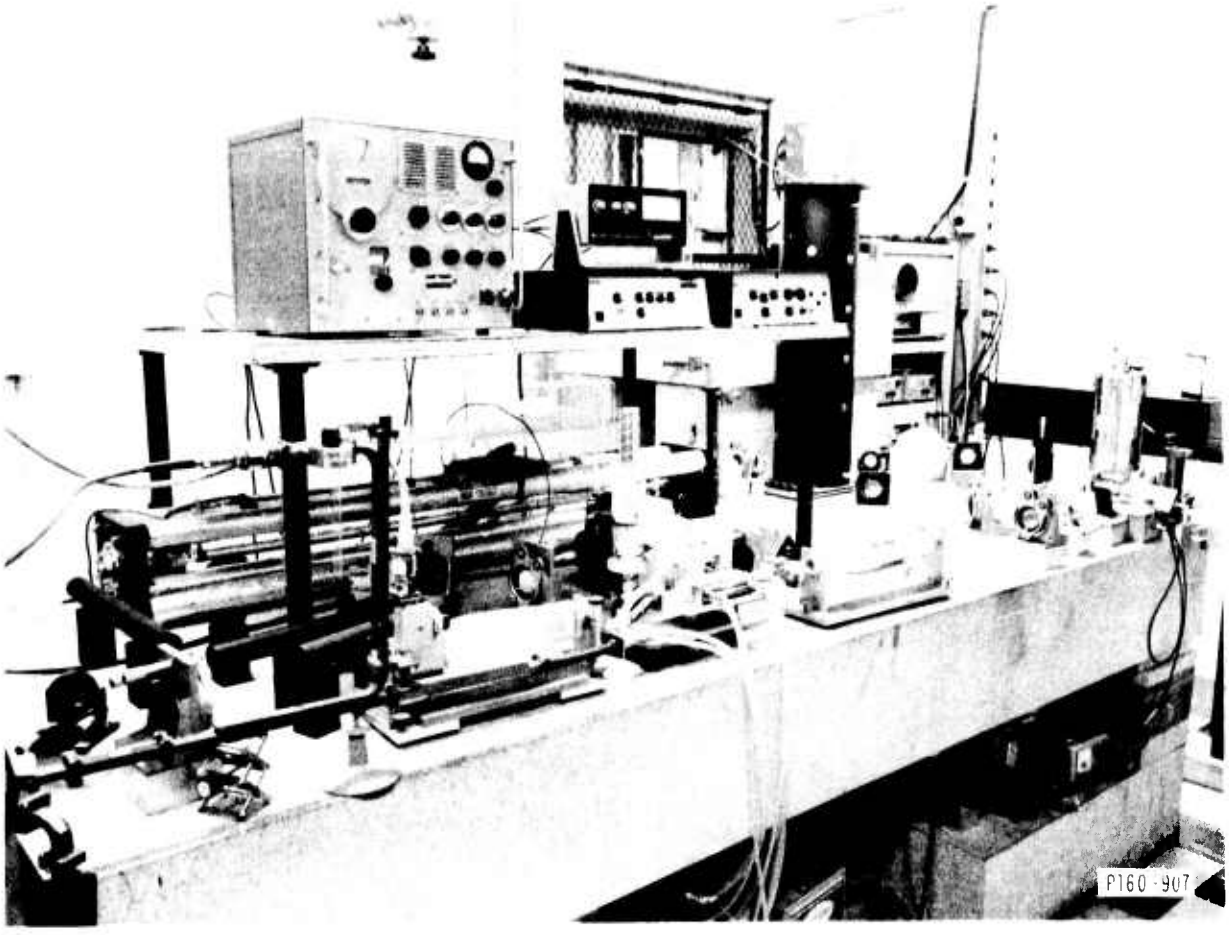

Fig. 7. Backscatter system optical bench.

ramp generator is constructed to make the 1 GHz chirp extremely linear. This is necessary to achieve the 15 cm range resolution (unweighted) by pulse compression. The linearity is such that the phase of the chirp varies by only 10° (peak-to-peak) during 1 GHz chirp.

The specifications of the generator are

PRF	100-3600 (2000 normally used)
Output Level	0 dBm
Output Level Variation	± 1 dB (maximum)

A self correlation provision in the generator allows the chirp phase to be constant from pulse to pulse. Although this feature is not used in the present system because the range is only 60 m, it would be necessary in the staggered chirp mode for long range operation.

The output of the ramp generator is mixed with a stable X-band klystron oscillator in a microwave diode upconverter to give the required 15.6 GHz output. This is amplified by a 100W TWT amplifier and is fed into the modulator via waveguide where the infrared and microwave fields mix. The present modulator increases the output level variation to ± 2 dB.

As explained in the Modulator Section the output of the modulator is a sideband orthogonally polarized in space to the carrier. A Germanium Brewster angle polarizer is used to extinguish the carrier. Due to imperfections in the polarizer and pressure induced birefringence in the modulator crystal the carrier can be reduced by about 17 dB (26 dB theoretical limit). The modulator output passes through a beamsplitter creating a signal path and a local oscillator path.

The local oscillator path contains a tunable Fabry Perot etalon which has 40 GHz free spectral range and a Finesse of 30, giving the desired 1 GHz band pass. This reduces the sideband carrier isolation further and selects the single sideband to be used in producing the radar signal. Figure 7 is a photograph of the optical components.

The signal path contains optics to adjust the output beam divergence in order to control the beam diameter at the target. Beam diameters from 7-100 cm at the target which is 60 m from the output mirror have been employed. The output mirror is electronically controlled to scan in a raster manner. The scan rate and step size are variable. The electronics also provide a sync pulse each time the position is changed. In this way the pulses can be continuously recorded and later reconstructed into angle-angle positions.

The return path is purposely separate from the output path to eliminate backscatter problems. The optics in the return path match the return Gaussian beam divergence to that of the local oscillator so that mixing can be optimized.[2]

The return is delayed by 400 nsec (for the 120 m round trip) relative to the local oscillator. For the 1 GHz chirp, 250 μsec pulse this gives a nominal 1.6 MHz difference in frequency between the LO and the return path. The mixing beam splitter combines the LO and the receive path.

The detector is a Ge:Cu photoconductor optimized for 2 MHz response. For the return signal frequency of the backscatter system photoconductors Ge:Cu is superior to HgCdTe photovoltaic detectors because of its superior (larger) shunt resistance which reduces the Johnson noise of the detector and its ability to withstand higher optical powers without damage.

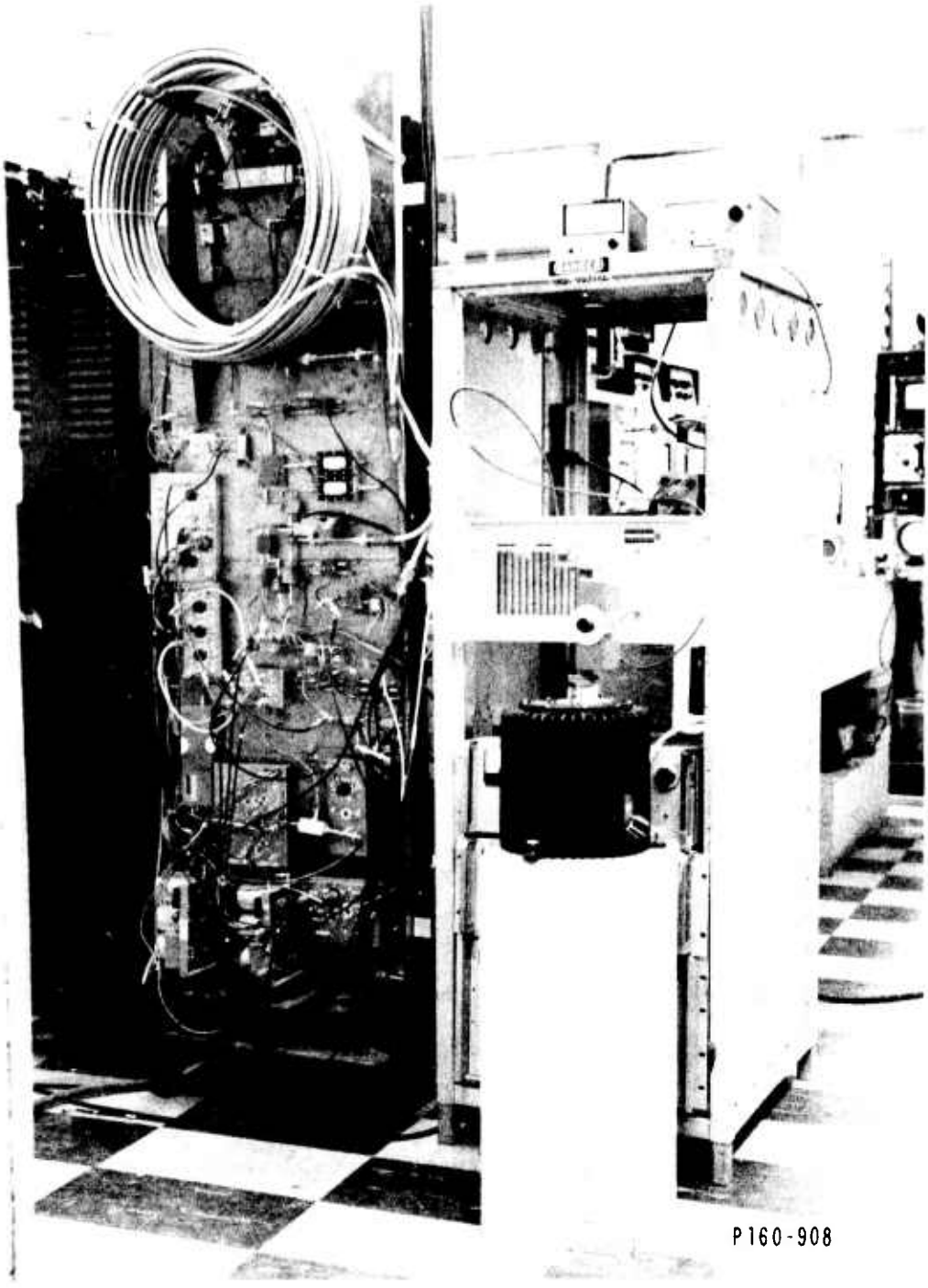

Fig. 6. Chirp waveform generator.

The mixed beam (LO and received) then modulates the detector output by the difference frequency, nominally 1.6 MHz. The resultant output of the detector is the radar signal. The 1.6 MHz, 250 μsec pulse has a constant starting phase from pulse to pulse unless there is target motion (intentional or induced by building vibrations).

In order to record the correlation detector output the 1.6 MHz carrier must be downconverted to match the 80 kHz bandwidth of a standard FM instrumentation recorder. This is accomplished by using a trigger pulse from the ramp generator to trigger a gated reference oscillator (GRO) whose frequency is 40 kHz offset from the correlation detector output. The GRO starts each 250 μsec burst at the same phase to avoid introducing phase errors into the doppler processing. The correlation detector and GRO are mixed and amplified to the optimum recorder level.

It is important to review the chain of events in the on-line data recording. The radar return is a 250 μsec pulse which when mixed with the LO and downconverted provides a nominal 40 kHz, 250 μsec sine wave. By recording the microwave trigger pulse (line sync) on the tape recorder as well as using it to trigger the GRO, we not only mark the beginning of the signal pulse, but we have carefully preserved the phase information in the signal. The frame sync pulses are recorded to mark each angle-angle position of the scan. If the radar is used in a non-scanning mode then the frame syncs are still provided (obviously the stepping motors are shut off) to mark a block of data for computer analysis. A fourth channel is recorded which provides the time of day. The time is used to run the off-line analysis.

The off-line processing consists of playing the tape on an A/D converter system which provides a digitized tape in IBM format for computer analysis.

The instrumentation recorder is similar to the on-line recorder. It uses 4 play back channels as outputs to a computer controlled A/D converter. The tape is recorded at 120 ips and played back at 15 ips to increase the effective sampling speed of the A/D. This allows 160-200 samples per signal pulse to be obtained.

The computer program that controls the digitizing process takes commands from a teletype terminal. The start and stop times are read from the time channel on the recorder. Once the start time is reached the next frame pulse triggers the digitizing process. The digitization begins with the next line (signal pulse) and continues for 40-50 pulses (a parameter previously typed into the digitizer). This series of digitized chirps forms 1 logical record stored in a buffer which is then read onto a digital tape recorder in IBM format. (Storage capacity of the digitizer is limited to 8000 total samples.)

III. SYSTEM SENSITIVITY

The desired sensitivity of the backscatter range is 0 dB signal-to-noise ratio on a -30 dBsm (10^{-3} m^2) target illuminated with a 1 m diameter beam at a 60 m range. This is equivalent to detecting a 10^{-2} m^2 resolution element with a 10% reflectivity. This section will discuss the theoretical and measured sensitivity to date and explore the alternatives to achieving the desired sensitivity.

The signal-to-noise ratio for heterodyne detection can be written as[3]:

$$\frac{S}{N} = \frac{i^2_{IF}}{i^2_n} \tag{1}$$

i^2_{IF}, the homodyned signal current, is

$$i^2_{IF} = [2\eta^2 G^2 e^2/(h\nu)^2]\ P_{LO} P_R K^2 \tag{2}$$

η, the external quantum efficiency of the Ge:Cu detector

G, the photoconductive gain

P_{LO}, P_R, the local oscillator and received signal power

K, the mixing efficiency

The noise terms are:

$$i^2_n = \frac{4e^2 G^2 \eta [P_{LO} + P_C] B}{h\nu} + \frac{4KT_L B}{R_L} \tag{3}$$

P_C, the carrier leakthrough power

B, the single range element bandwidth, 4 kHz

T_L, R_L, the effective Johnson noise temperature and resistance

P_T, transmitted signal power

Present system sensitivity allows a single pulse return of 27 dB ±3 dB on a Lambertian scatterplate with 7 cm diameter beam (σ = -20 dBsm) and 80 dB ±3 dB on a retroreflector (σ = 32 dBsm).

The significant existing system parameters are:

P_{Laser} = 50 W

$P_{\mu wave}$ = 80 W

$P_{Sideband}$ = 30 mw

P_{LO} = 9 mw (after beamsplitter 30%)

= 3 mw (after Fabry-Perot)

= .9 mw (at detector)

P_C = 750 mw (after beamsplitter) polarization different

= 30 mw (after Fabry-Perot) from LO

= 15 mw (at detector)

P_T = 21 mw (after beamsplitter 70%)

There is a second 70% beamsplitter on the received path so the effective received power has an additional 30% loss. The optical reflection loss from 12 surfaces provides an optical transmission path loss of 20%.

The two principle noise sources for the system are the LO shot noise and the unmodulated carrier leakthrough, P_C, shot noise. The resultant signal-to-noise ratio is

$$\frac{S}{N} = \frac{[2\eta^2 G^2 e^2/(h\nu)^2] P_{LO} P_R K^2}{4e^2 G^2 \eta (P_C + P_{LO}) B/h\nu} = \frac{\eta P_{LO} P_R K^2}{2h\nu (P_C + P_{LO}) B} \qquad (4)$$

The minimum detectable power is therefore:

$$P_{R_{min}} = \frac{2h\nu (P_C + P_{LO}) B}{\eta P_{LO} K^2}$$

Using the previously provided system parameters and $\eta = 30\%$

$$P_{R_{min}} = \frac{8.8 \times 10^{-15} W}{K^2}$$

This compares to $P_{R_{min}} = 2h\nu B/\eta = 5.3 \times 10^{-16} W$ in the quantum limit when $K = 1$. For the $\sigma = -20$ dBsm (S/N = 27 dB) scatterplate the power received is related to the power transmitted by:

$$P_R = \frac{P_T, 4\pi A_R^2 \sigma}{(4\pi R^2)^2 \lambda^2} = 4.2 \times 10^{-9} P_T,$$

where A_R is the effective receiver area.

Taking into account the receiver beamsplitter and optical transmission effects, the effective power transmitted is:

$$P_T, = .56\ P_T = 12\ mw$$

Therefore

$$P_R = 5.1 \times 10^{-11} W$$

The signal to noise ratio on the $\sigma = -20$ dBsm target is therefore

$$\frac{S}{N} = \frac{5.1 \times 10^{-11}}{8.8 \times 10^{-15}/K^2} = K^2\ 5.8 \times 10^3 = (38 + \log K^2)\ dB$$

The experimental results show the scatterplate has a signal to noise of 27 dB indicating that the combined mixing efficiency and system loss is about -11 dB. This is a realistic number considering the number of optical elements in the system.

Expanding the beam from 7 cm to 100 cm diameter requires that the effective transmit/receive area be reduced by $(7/100)^2$. Since the system sensitivity is proportional to A_T^2, system sensitivity is reduced by $(7/100)^4$ or 46 dB. For the system numbers just described the minimum detectable cross-section, σ_{min}, is reduced from $\sigma_{min\ 7\ cm} = -47$ dBsm to $\sigma_{min\ 100\ cm} = -1$ dBsm.

Since the desired sensitivity of the system is 0 dB on a $\sigma = -30$ dBsm element with a 100 cm diameter beam, a 29 improvement in sensitivity is needed.

A. System Improvements

Using the last analysis the effect of three possible increases in the sideband power level and their effect on the system sensitivity are explored. 1) The use of CdTe crystals. This will increase the sideband power by 6 dB. This development is currently in progress. 2) The use of a 10 dB optical amplifier. We have a prototype optical amplifier which has been built by Hughes Research Laboratory (Malibu). Hughes has successfully operated the amplifier at various gains and pressure levels. The pressure and gain theoretically determine the bandwidth of the optical amplifier. It is hoped that 10 dB of gain can be obtained with a bandwidth of 500 MHz (3 dB)

from the prototype amplifier. From Hughes' data this appears to be possible. As mentioned in Section IIB an isotope laser will have to be used to produce the sideband so that it can be amplified. This laser is currently being developed to produce power levels near 50 W. 3) a 20 dB optical amplifier may become available in the future from Hughes (Culver City). It has been constructed but no significant measurements have been made. It is intended for future use in the backscatter system.

Case 1 - Effect of 6 dB Increase in Sideband by Use of CdTe Modulator Crystals.

This will increase P_{LO} from .9 mw to 3.6 mw and P_T, from 12 mw to 48 mw while P_C remains fixed at 15 mw. The result will be to reduce P_{Rmin} from 1.1×10^{-13} W to 2.8×10^{-14} W and increase sensitivity by 11 dB because while both P_{LO} and P_R are increased by 6 dB in Equation 4, the denominator increases only slightly. Thus 11 dB of the needed 29 dB can be achieved improving the modulator efficiency. 18 dB gain is still needed.

Case 2 - 10 dB Optical Amplifier

For this case, again, P_{LO} is increased from 3.6 mw to 36 mw and P_T, from 48 mw to 480 mw. P_{LO} is now greater than, but comparable to P_C at 15 mw. The numerator of Equation 4 increases by 20 dB while the denominator increases by 4 dB (due to $P_{LO} + P_C$) leaving a net gain in sensitivity of 16 dB. P_{Rmin} is reduced to 9.5×10^{-15} W (i.e., compared to 6.7×10^{-15} W for the quantum limit case).

The total sensitivity improvement for Case 1 and 2 is 27 dB. This improvement will allow a 0 dB signal-to-noise ratio on a -28 dBsm target. This is 2 dB less sensitivity than the minimum desired result.

Case 3 - 20 dB Optical Amplifier

In this case P_{LO} is increased from 3.6 mW to 360 mW. This is a much greater LO power than is needed (or even desired) to achieve a quantum noise limit. This power can be reduced by decreasing the reflectivity of the beamsplitters. In any case quantum noise limit is achieved, that is,

$$P_{R_{min}} = 6.7 \times 10^{-15} \text{ W}$$

P_T, is increased from 48 mW to 4.8 W (possibly more if the beamsplitters are changed). The net gain in sensitivity (over Case 1 improvement) is 27 dB. That is, a +9 dB signal-to-noise ratio can be achieved on a -30 dBsm target (σ_{min} = -39 dBsm). This will provide the full desired sensitivity. Table II summarizes the results.

To achieve the minimum desired sensitivity we are constructing the CdTe modulator and making the prototype optical amplifier operational for the backscatter range. The optical amplifier built by Hughes, Culver City, will be tested independently from the backscatter program and made operational in the system when its performance is deemed satisfactory.

IV. DATA PROCESSING AND ANALYSIS

The digitized output from the correlation detector is read onto the disc of the IBM 370. The data are organized in units of lines and records as previously discussed. Each line represents the sampled digitized response of a single chirp. Each record represents a sequence of chirped signals. For the case of a single point target the functional form of each line is a single frequency sinusoid of 250 μsec duration. The unweighted

TABLE II

Case	Beam	σ_{min}	Scatterplate[1] 30 cm x 30 cm σ	Scatterplate[1] 30 cm x 30 cm S/N	Sideband Power	$P_{R_{min}}$	$P_{T'}$
4/01/76	7 cm	-41 dBsm	-20 dBsm	21 dB	10 mw	1.1×10^{-13}W	4×10^{-3}W
4/01/76	100 cm	+5 dBsm	-8 dBsm	-13 dB	10 mw	1.1×10^{-13}W	4×10^{-3}W
4/30/76 50W Laser	7 cm	-47 dBsm	-20 dBsm	27 dB	30 mw	1.1×10^{-13}W	1.2×10^{-2}W
50W Laser	100 cm	-1 dBsm	-8 dBsm	-7 dB	30 mw	1.1×10^{-13}W	1.2×10^{-2}W
6 dB Modulator Improvement	100 cm	-12 dBsm	-8 dBsm	4 dB	120 mw	2.8×10^{-14}W	4.8×10^{-2}W
Modulator + 10 dB Amp	100 cm	-28 dBsm	-8 dBsm	20 dB	1.2 W	9.5×10^{-15}W	4.8×10^{-1}W
Modulator + 20 dB Amp	100 cm	-39 dBsm	-8 dBsm	31 dB	12 W	$6.7 \times 10^{-15*}$W	4.8 W

$P_{R_{min}}$ = minimum detectable power (at the detector)

$P_{T'}$ = effective transmitted power (includes beamsplitter losses in Transmit and Receive Path)

*quantum noise limit (including system losses)

(1) present calibration target

Fourier transform of the time domain output results in spectral display in the frequency domain. The functional form in the frequency domain is sin x/x. The frequency spectrum is then directly converted to range information using the conversion of 4 kHz to 15 cm. The sin x/x function has sidelobes 4 kHz wide at 13 dB below the central peak. To improve the dynamic range of the system these sidelobes can be reduced by "Hamming" weighting the time domain samples by a cosine function. The result is that the central lobe is widened by 40% thereby reducing the range resolution from 15 cm to 25 cm, but the sidelobes and therefore the dynamic range of the system is theoretically improved from 13 dB to 40 dB (25-30 dB in practice). Figure 8 shows the theoretical spectrum of the $(\sin x/x)^2$ waveform before and after Hamming weighting.

To obtain doppler information a second transform is required for each range (frequency) bin. The transform requires a sequence of consecutive lines, the length of the sequence determining the doppler resolution. The output of the two dimensional transform, which represents a single aspect-angle image of the target, is then displayed. Figure 9 shows a block diagram of the major steps in the range-doppler processing.

The unambiguous doppler is 2 kHz which is determined by the pulse repetition frequency. The doppler resolution is determined by the total number of chirps (lines) used in the second FFT. The doppler resolution is

$$\Delta f_D = \frac{2 \text{ kHz}}{N}$$

where N is the number of chirps in the second FFT.

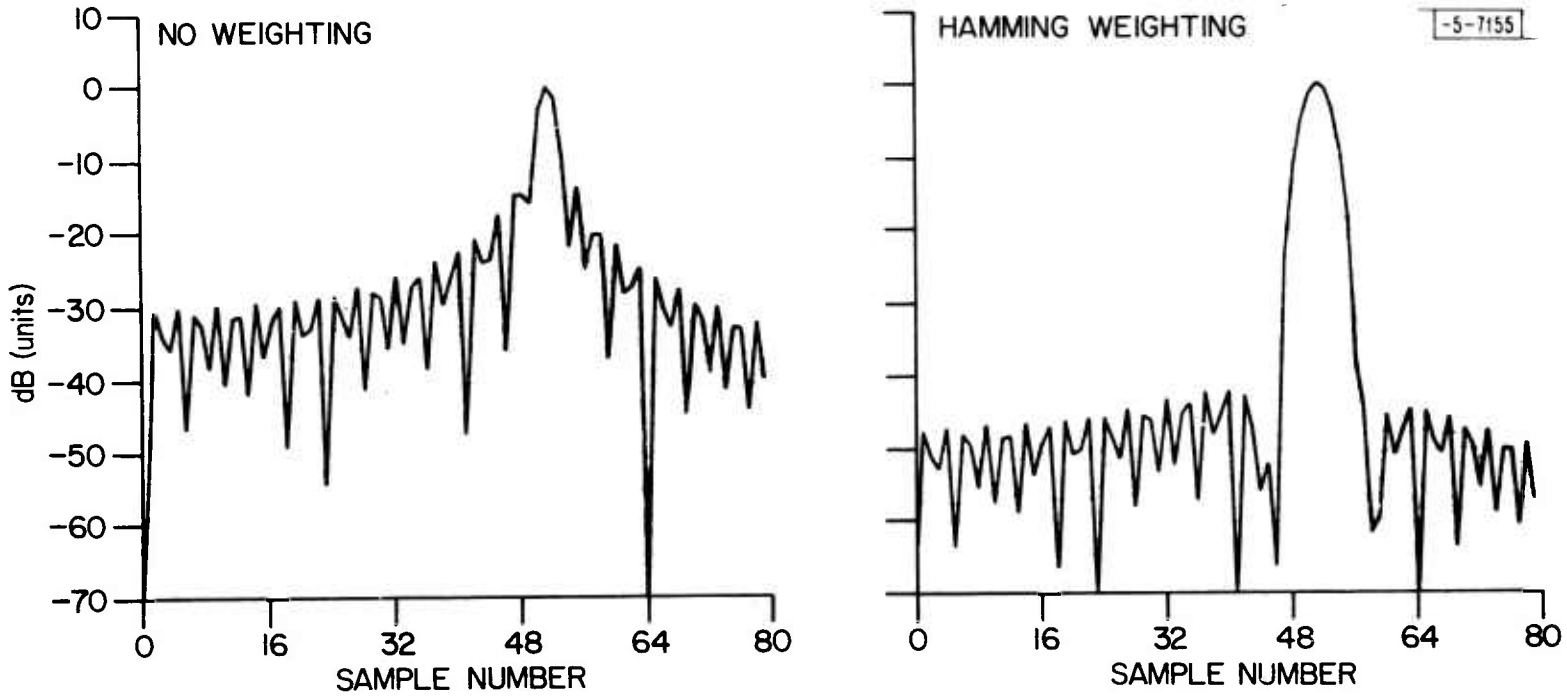

Fig. 8. Sin x/x spectrum without and with Hamming weighting.

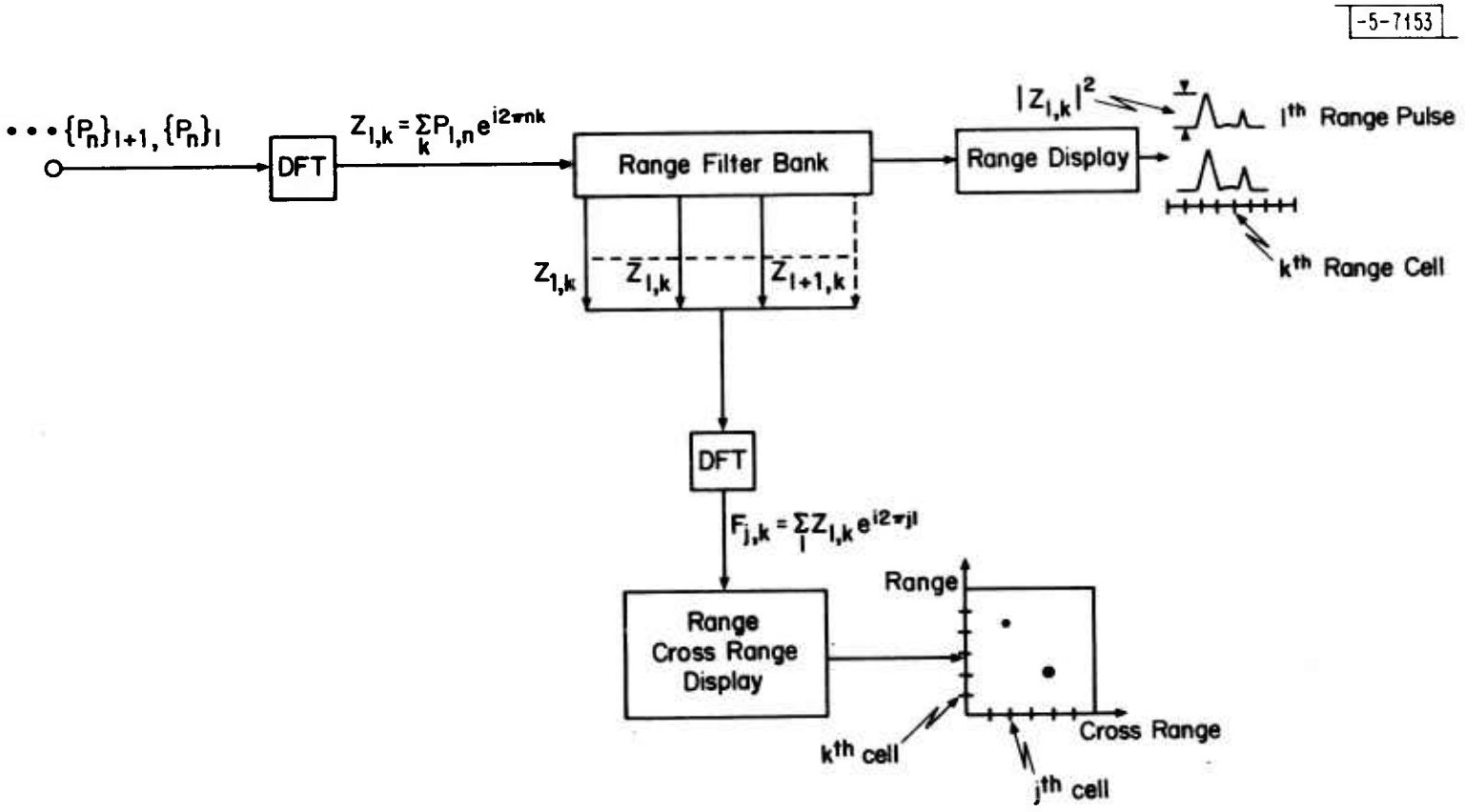

Fig. 9. Processing block diagram.

The crossrange resolution therefore is

$$\Delta x_{res} = \frac{\lambda \Delta f_D}{2\omega_r}$$

Table III summarizes the backscatter system signal and imaging parameters.

V. EXPERIMENTAL RESULTS

This section will describe the significant results obtained with the wideband 10.6 μm backscatter range. It must be pointed out that these results were intended to demonstrate the range and doppler imaging capabilities of the backscatter system and not to represent signatures of targets that are of strategic or even real interest.

The real time output of the correlation detector has been previously described as a 250 μsec frequency burst. Figure 10 shows an oscilloscope photograph taken with a 1/30 sec exposure of a retroreflector target. Since the correlation detector frequency is proportional to the range of the return when returns are received from different ranges the 250 μsec burst consists of the sum of the different frequency components. Figure 11 shows the time-domain return of two retroreflectors separated in range by 50 cm.

A. Range-Doppler Resolution

The theoretical range resolution for a 1000 MHz waveform and two equal amplitude point targets is 15 cm. The real time returns from two retroreflectors located at 60 m separated by 15 cm in range are clearly discernible in the frequency domain plot shown in Figure 12.

TABLE III

SIGNAL AND IMAGING PARAMETERS

Pulse Duration	T	250 μsec
Interpulse Spacing	T'	500 μsec
Bandwidth	W	1000 MHz
Target Rotation	ω	.01 rad/sec

Frequency Domain			Spatial Domain		
Frequency Resolution: (unweighted)	$\Delta f = \frac{1}{T}$	4 kHz	Range Resolution: (unweighted)	$\Delta r = \frac{C}{2W}$	15 cm
Dynamic Range: (unweighted)	13 dB (theoretical and experimental)				
Frequency Resolution: (Hamming weighted)	Δf_H	6 kHz	Range Resolution (Hamming weighted)	Δr_H	25 cm
Dynamic Range: (Hamming weighted)	40 dB (theoretical), 25 dB (experimental)				
Doppler Resolution:	$\Delta f_D = \frac{1}{NT'}$	.2 kHz (N = 10)	Crossrange Resolution:	$\Delta x_D = \frac{\lambda \Delta f_D}{2\omega}$	10 cm
Unambiguous Doppler Interval:	$f_D = \frac{1}{T'}$	2 kHz	Unambiguous Crossrange:	$x_D = \frac{\lambda f_D}{2\omega}$	100 cm

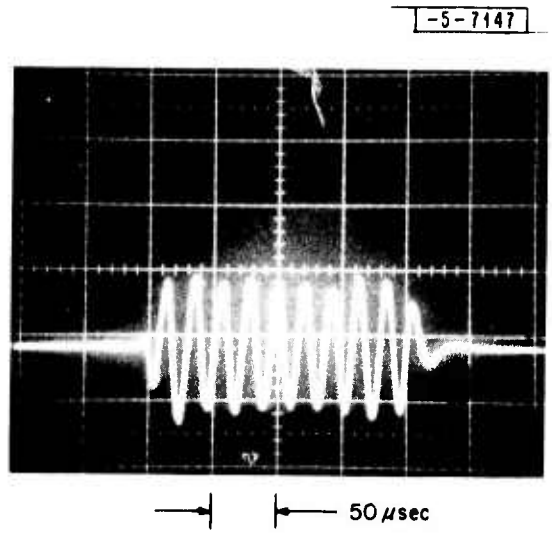

Fig. 10. Downconverted correlation detector output of a single retro.

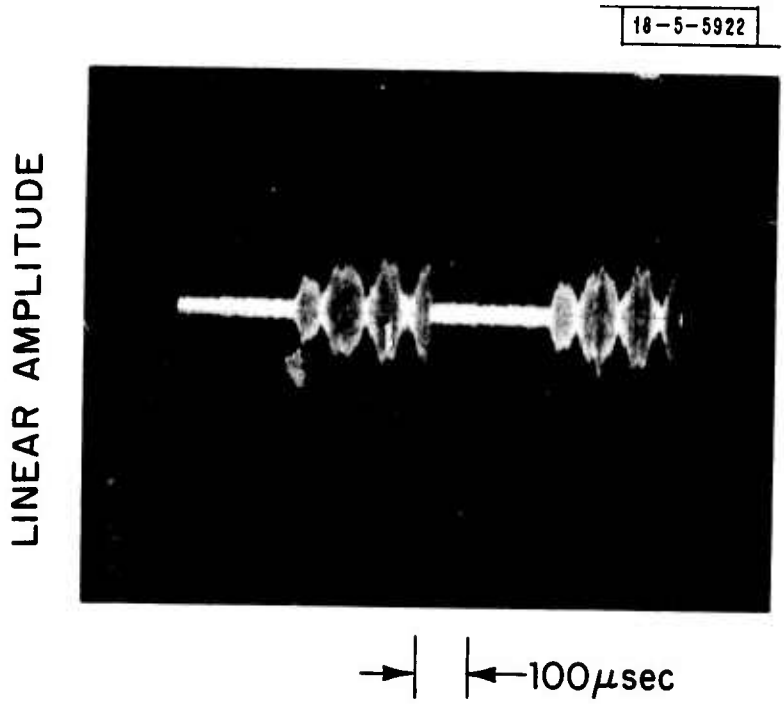

Fig. 11. Correlation detector otuput of two retros separated in range.

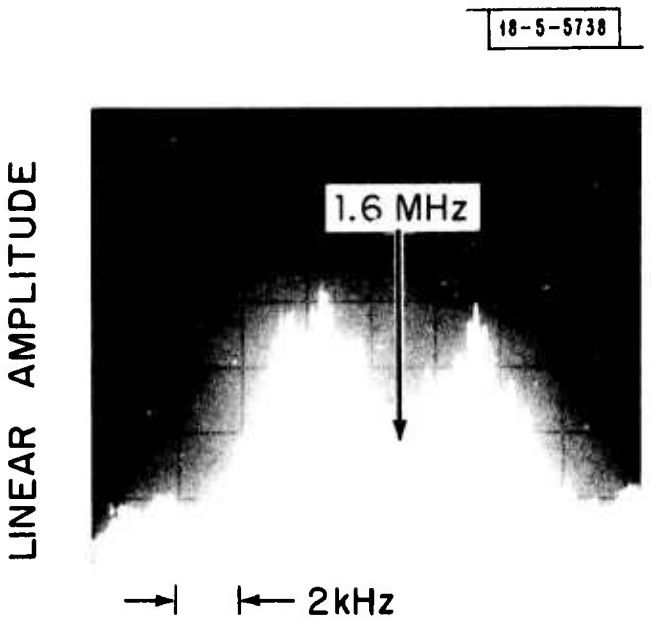

Fig. 12. Spectrum of correlation detector showing the 15 cm theoretical range resolution.

The doppler resolution is dependent on the number of chirp waveforms used in the second Fourier Transform as well as the system coherence time. The resolution can be increased with increasing number of chirps only as long as the system remains coherent. Figures 13 and 14 show the down-converted computer processed time waveform plots of consecutive chirps for single and double targets. Figure 15 shows the range-doppler image for two stationary (zero doppler) point targets as the number of chirp waveforms in the second transform is increased. Figure 15b shows doppler resolution improvement from 60 Hz to 30 Hz as more chirp waveforms are used. Figure 15c shows the degradation when additional chirps are used that are no longer coherent. The phase changes from chirp to chirp (with stationary targets chirp to chirp phase should be identical, see Figure 13) and manifests itself as an apparent (erroneous) doppler.

The coherence time of the system was determined to be in 30-50 msec range for the present outdoor range. In order to determine the equipment limitation on system coherence a 20 m gas cell (a small optical device that by means of many internal reflections has an optical path of 20 m) was installed on the optical bench, a retro placed at the output and the signal detected. The total optical path length was 40 m. System coherence time was substantially increased to greater than 500 msec. Figure 16a shows a photograph of the time waveform taken with a 500 msec exposure (integration). The phase coherence is clearly visible. Since the outdoor range coherence time is much less than this, (see Figure 16b with a 1/30 sec exposure) the limiting factors must be either target vibration or atmospheric turbulence. The mount is currently being instrumented to measure the target mount vibration.

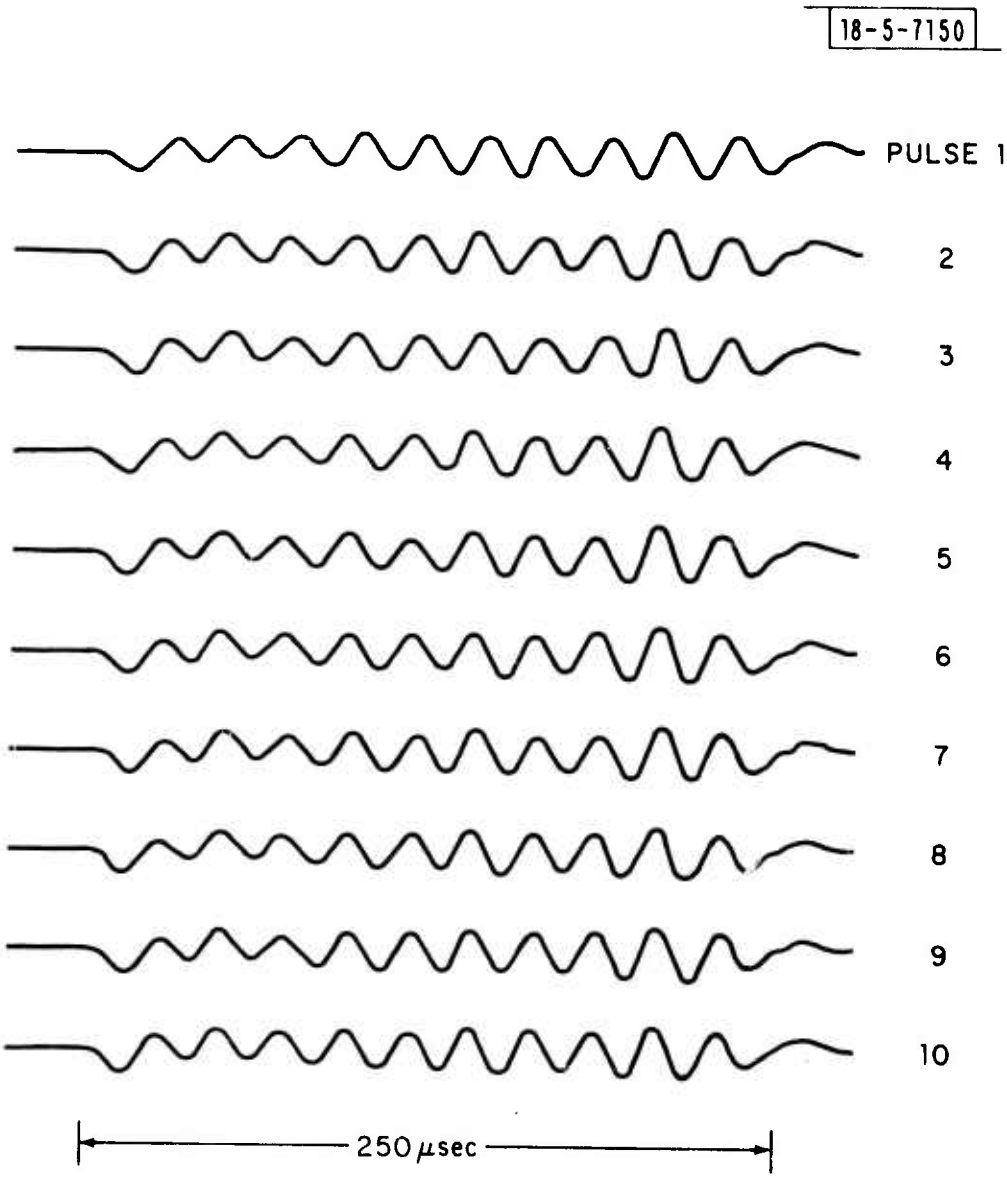

Fig. 13. Computer display of 10 consecutive returns from a stationary retro.

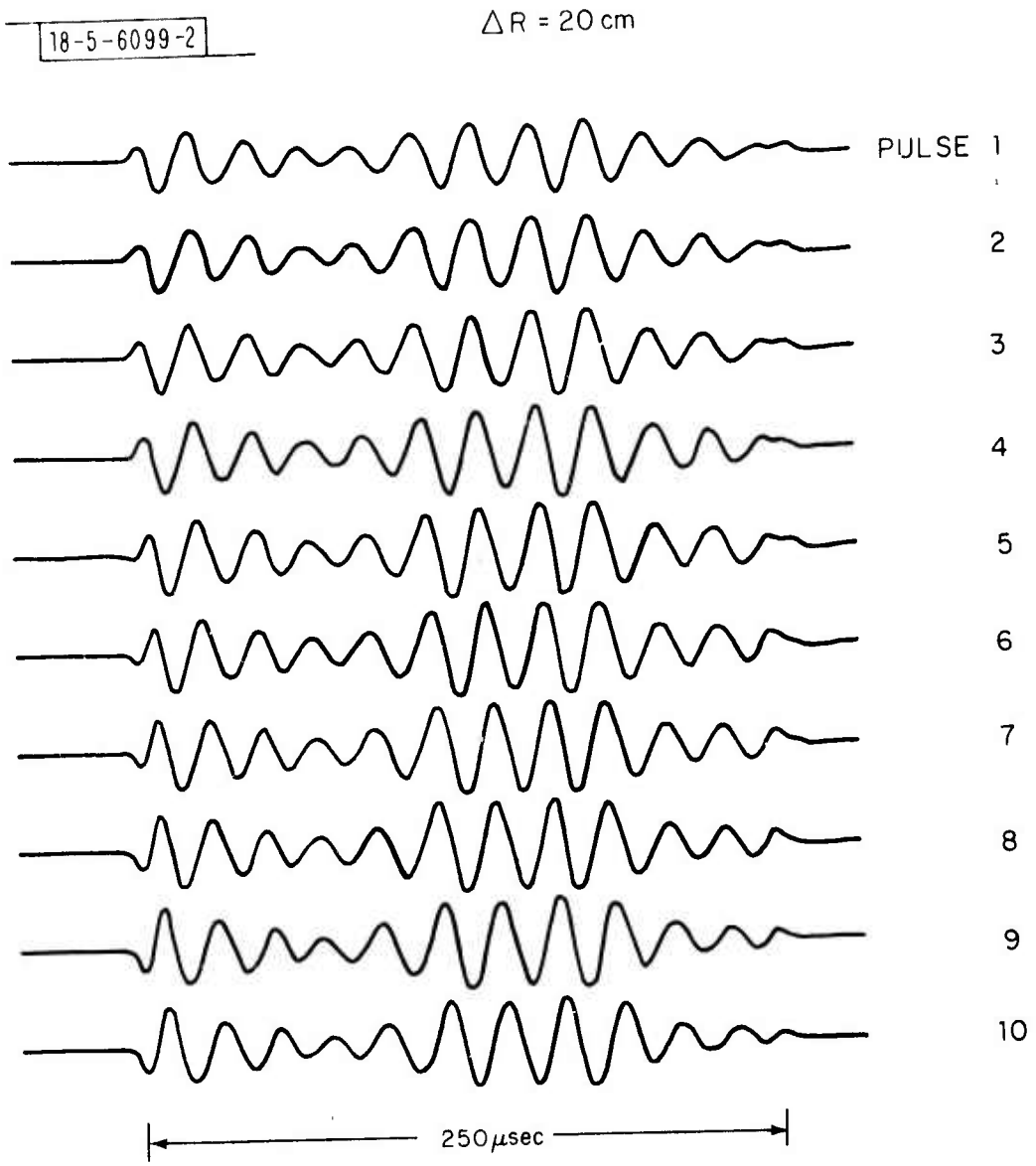

Fig. 14. Computer display of 10 consecutive returns from two stationary retros.

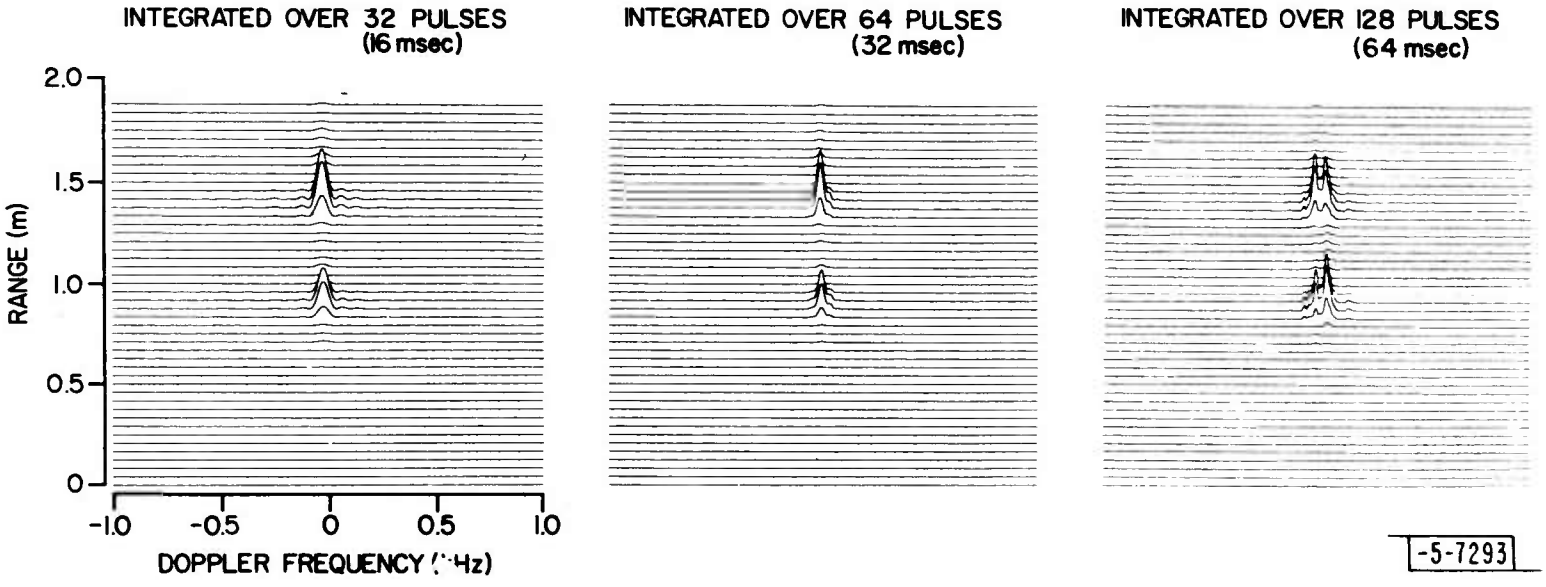

Fig. 15. Range-doppler image of two stationary retros showing the effect of increased processing time.

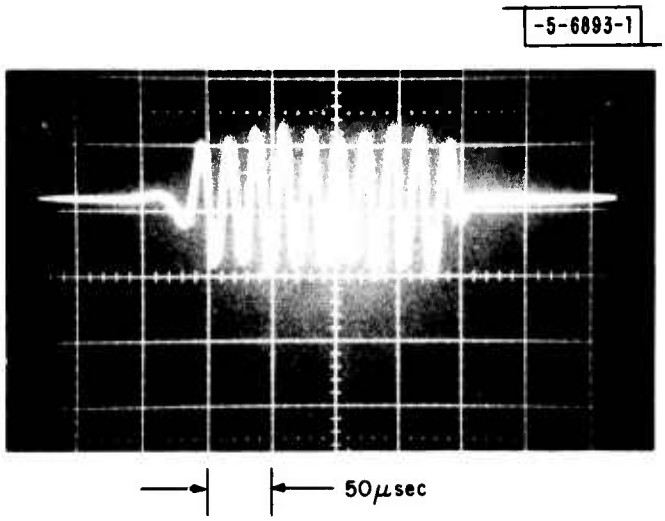

Fig. 16a. 1/2 second exposure of downconverted correlation detector output on indoor range.

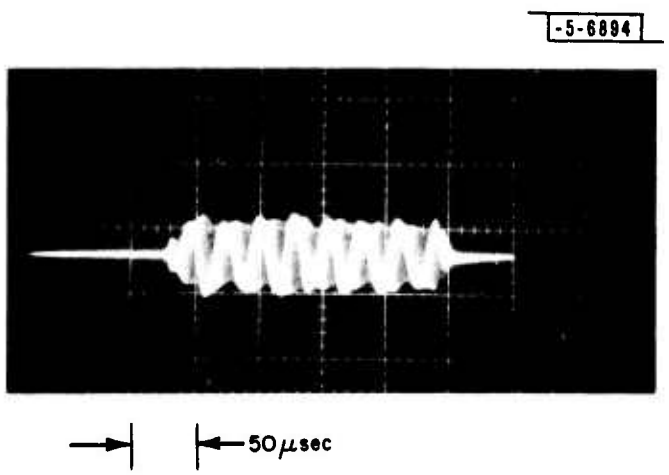

Fig. 16b. 1/30 second exposure of downconverted correlation detector output on outdoor range.

B. Range-Resolved Angle-Scanned Imaging

The first type of imaging described (see Section II) relied on a beamwidth much smaller than the target and the angle-angle position of the scanner to determine the crossrange dimension. The range for each angle-angle element is determined from the frequency information in each correlated chirp return.

To demonstrate the range-crossrange imaging capability of the wideband waveform a "V" shaped array of retroreflectors was assembled at the 60 m range. The separation between retros was 25 cm. Figure 17 shows the array as seen from the radar. Figure 18 shows a close-up view of the array. The radar was scanned across the array and the data recorded and processed. Figure 19 shows the resultant image when the angle-angle information of the scanner has been converted to crossrange.

To demonstrate this target contouring ability on an extended target an aluminum model of a rocket body was placed on the 60 m range and rotated at a 25° angle from rocket body normal (broadside) to the radar. This was done so there would be a range difference between the noise and tail of the target. Figure 20 shows the model as seen from the radar. The model was made of rough turned aluminum and presented a return with a bright "specular" at broadside (i.e., at normal incidence to rocket body) and a monotonically decreasing "diffuse" return as the angle between the rocket body normal and the radar increased. Figure 21 shows a contour plot of the returns in range and crossrange. The crossrange information again is determined by the angle-angle position of the scanner. The schematic of the rocket body is superimposed at the same angle as in the experiment to show

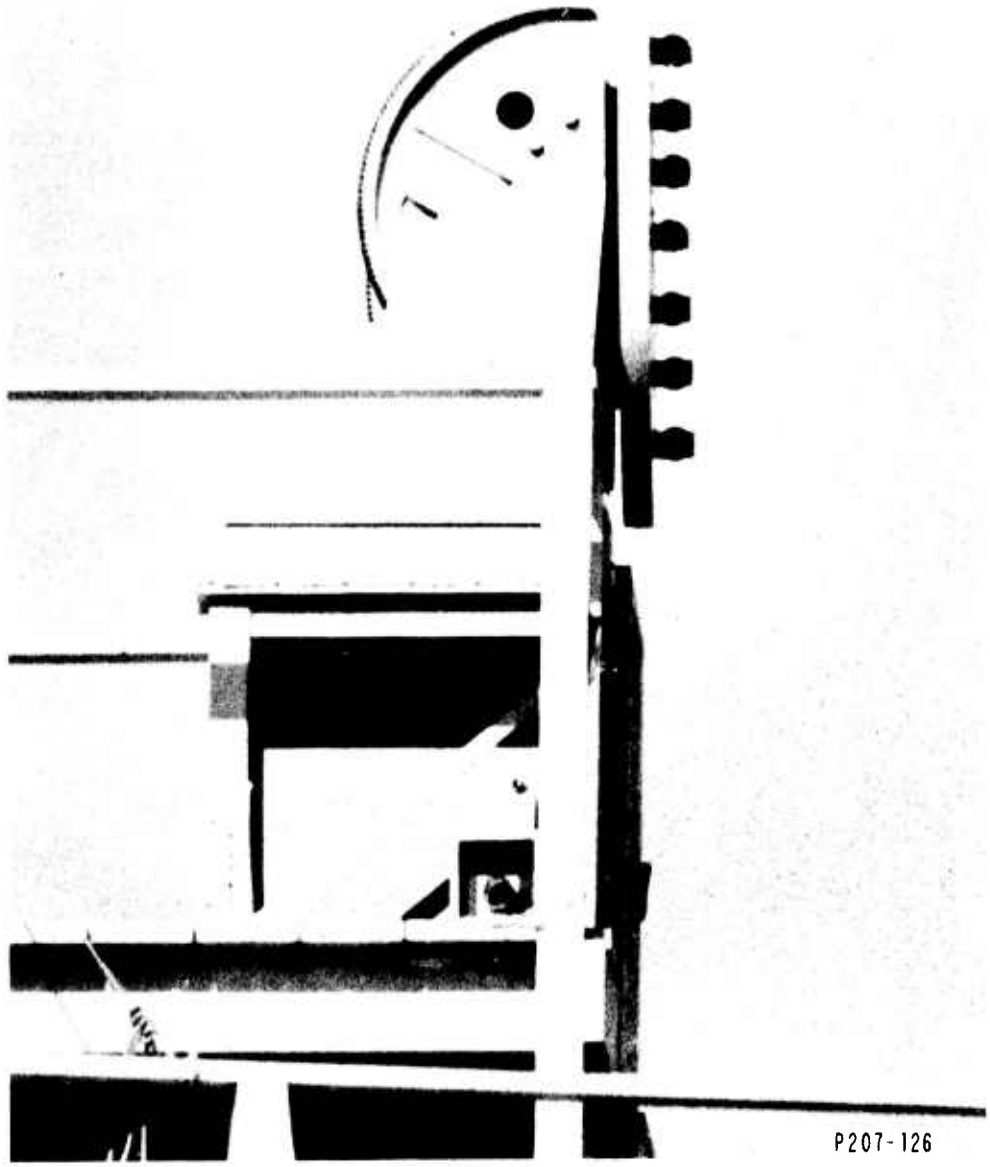

Fig. 17. Retro array as viewed from the radar.

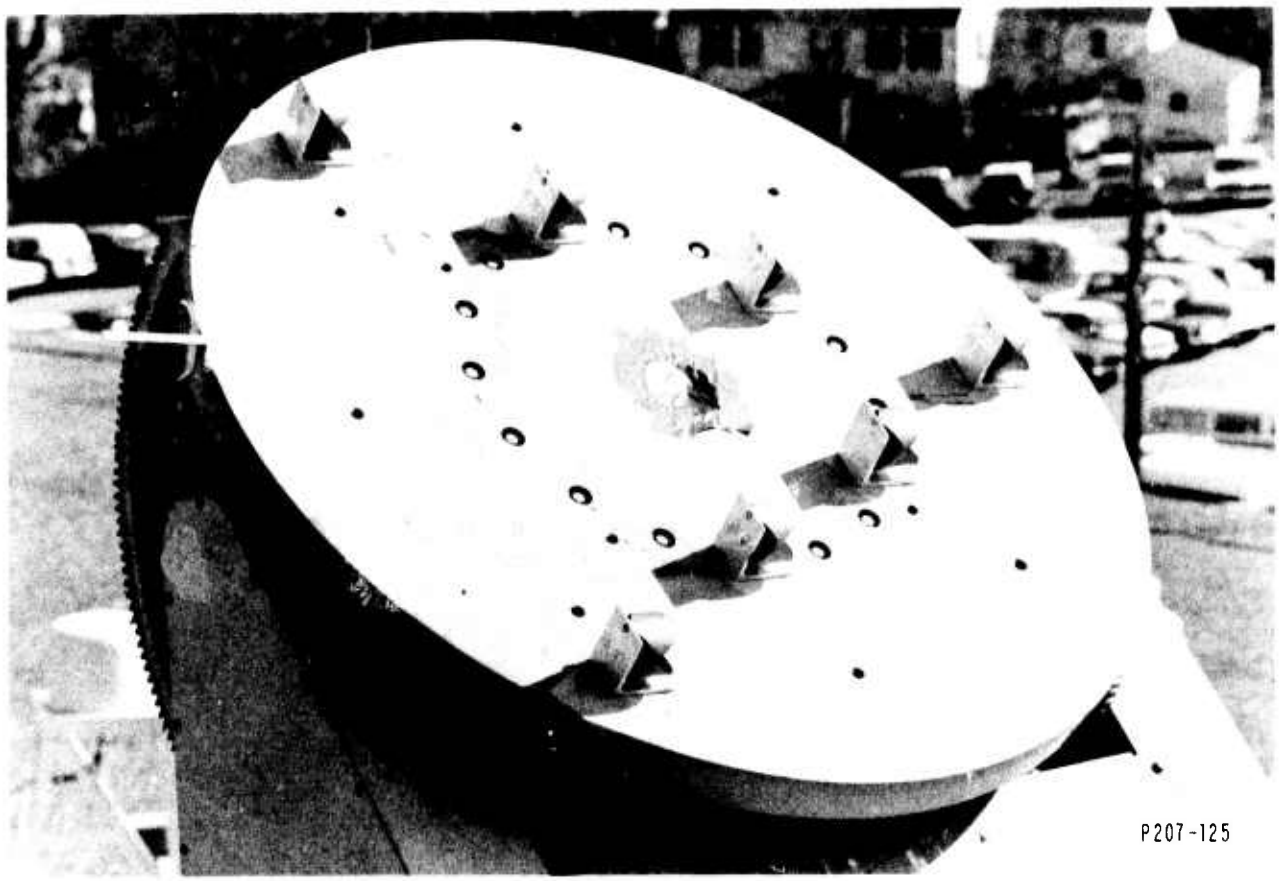

Fig. 18. Closeup of array.

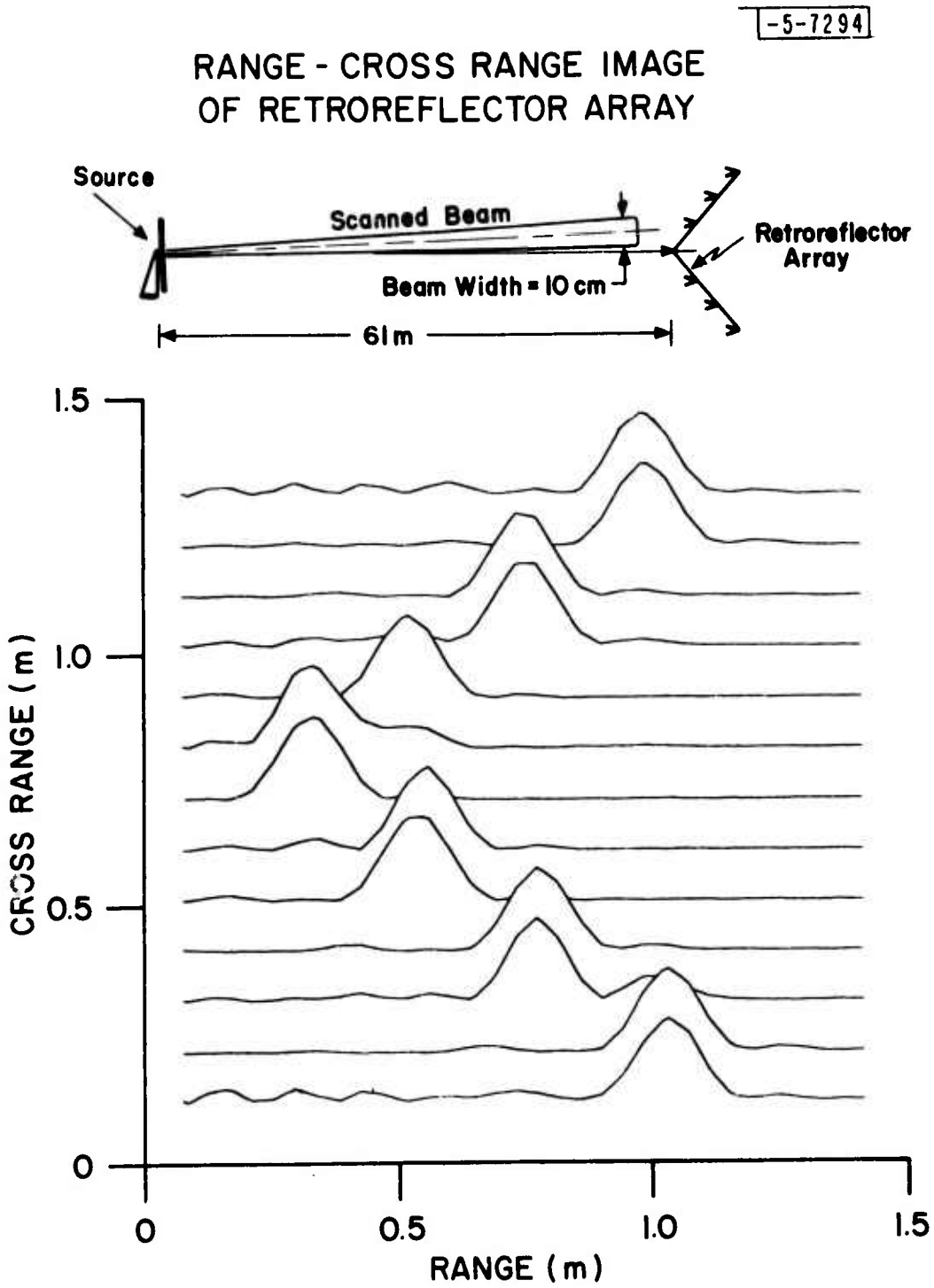

Fig. 19. 10.6 μm range-crossrange image of retro array.

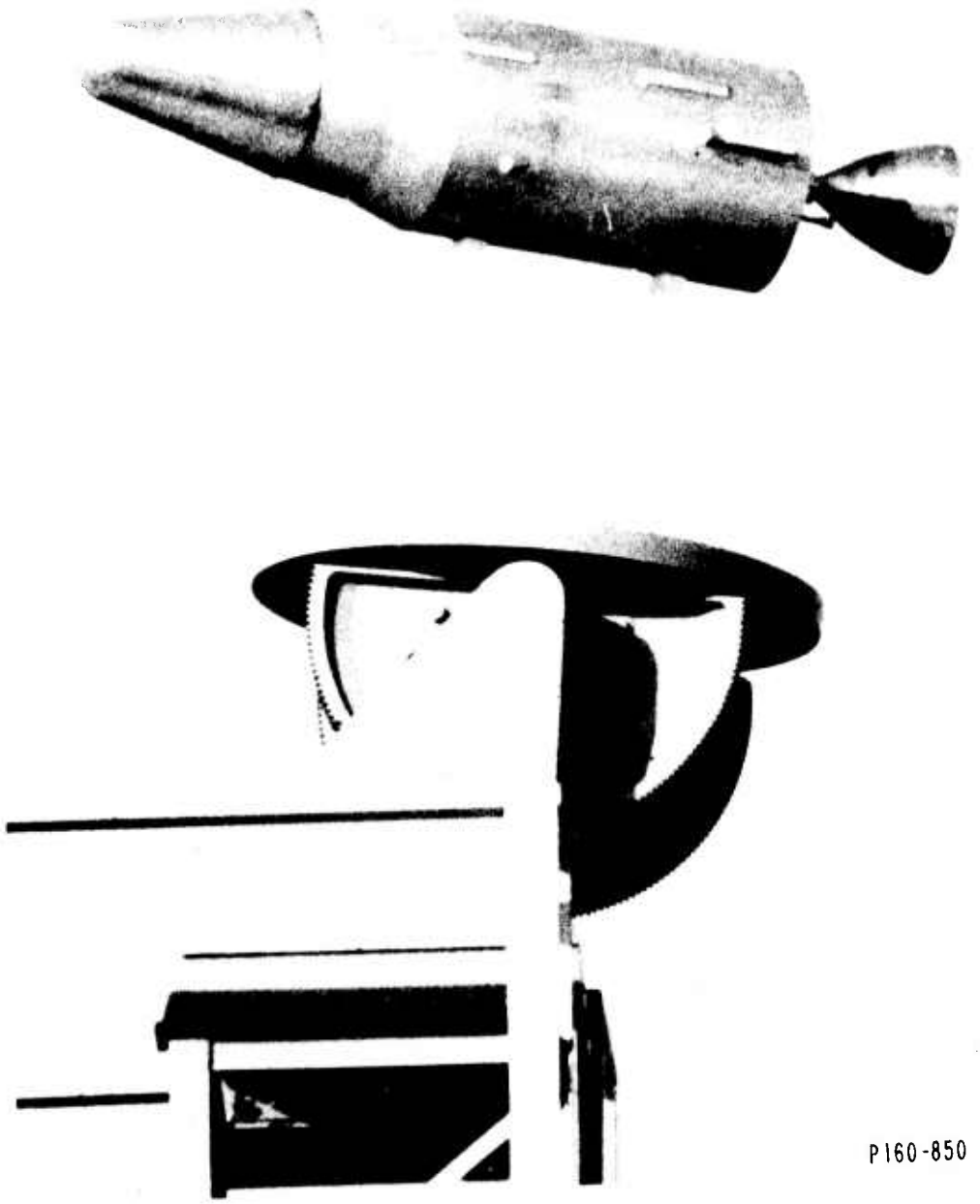

Fig. 20. Model rocket body as seen from the radar.

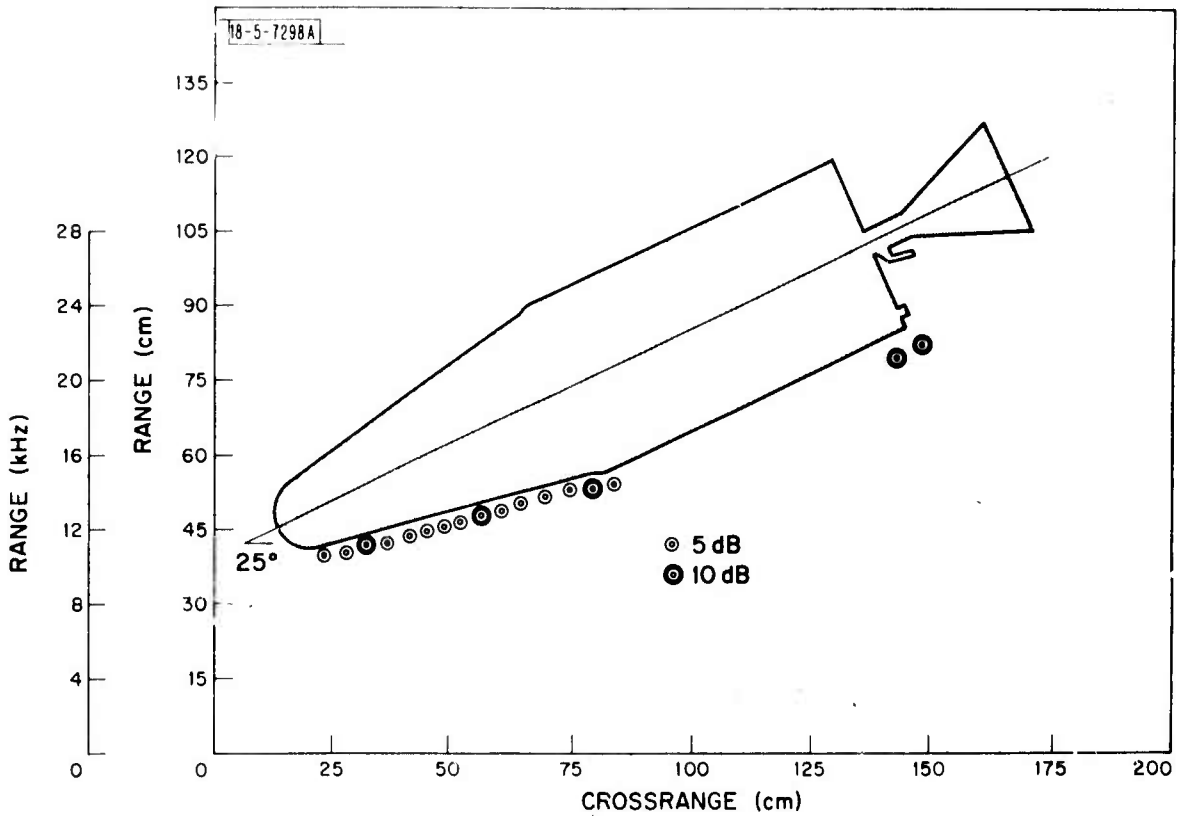

Fig. 21. 10.6 μm range-crossrange image of rocket model (Contour Plot).

that the returns follow the contour of body. The radar in Figure 21 is located at the bottom of the page and is propagating toward the top of the page. The returns from the noise section which is only 10° away from broadside are stronger than the returns from body which is 25° from broadside. Bright returns are seen at welded joints on the noise cone and edges near the tail. Figure 22 shows the results after a 6 dB improvement was obtained by non-coherent averaging techniques. Returns from the body proper are now clearly discernible. The complete reconstruction of the image requires the superposition of many different images (of which Figure 21 is an example) as described in Figure 3.

C. Range-Doppler Imaging

Range-Doppler Imaging was carried out using a 60 cm diameter beam at the 60 m range. Figure 23 shows the range-doppler image of a single moving retroreflector. The doppler resolution time was 8 msec (16 pulses). Figure 24 shows the range-doppler image of two retros; one stationary, the other moving toward the radar.

A rotary beam was constructed with retroreflectors at each arm. The retros were attached to the beam in a planetary fashion so that they always faced the radar. Figure 25 shows the range-doppler image when the retros were at maximum crossrange separation. Figure 26 shows a sequence of four views of the retros at different points in their rotation. The crossrange resolution of these images is approximately 15 cm. These images represent the first high resolution range-doppler images made at 10.6 μm. Figure 27 shows the various displays used to generate a two dimensional image of the rotating retroreflectors. The first image is a gray scale display where

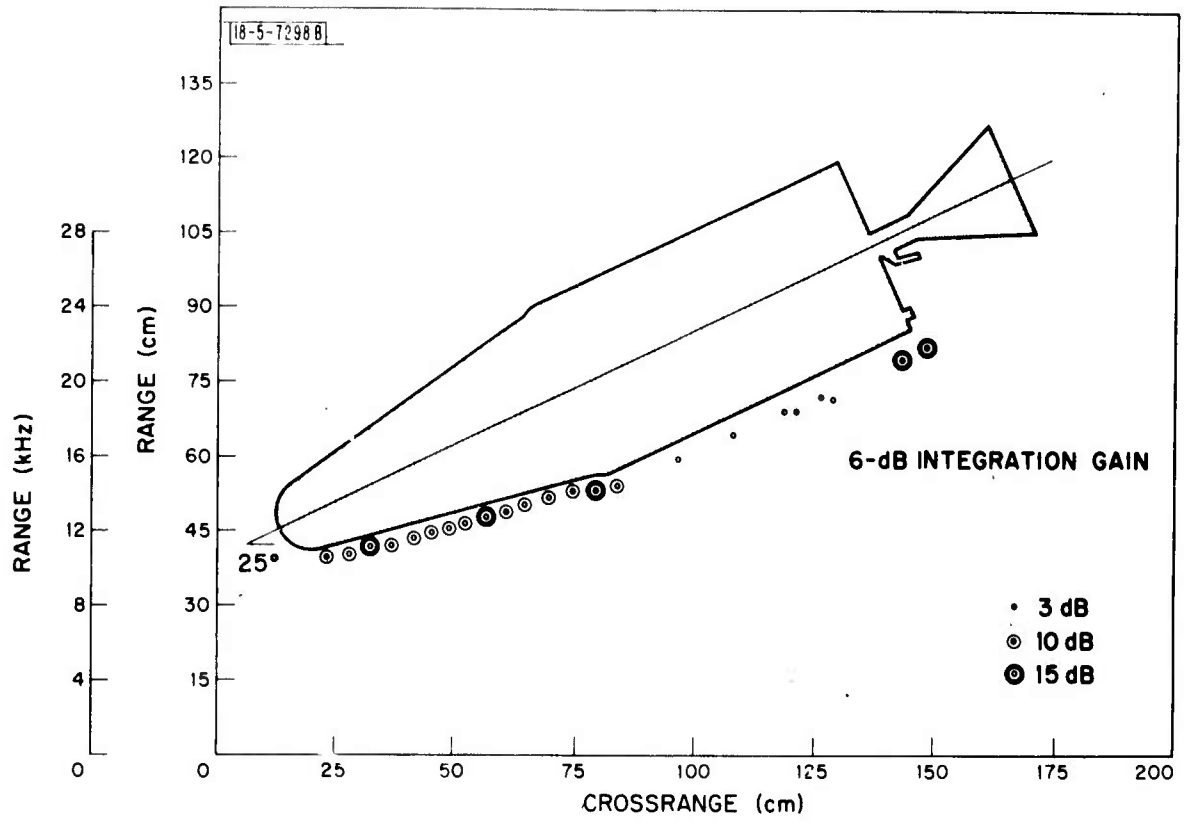

Fig. 22. 10.6 μm range-crossrange image of rocket model (Contour Plot with computuer averaging).

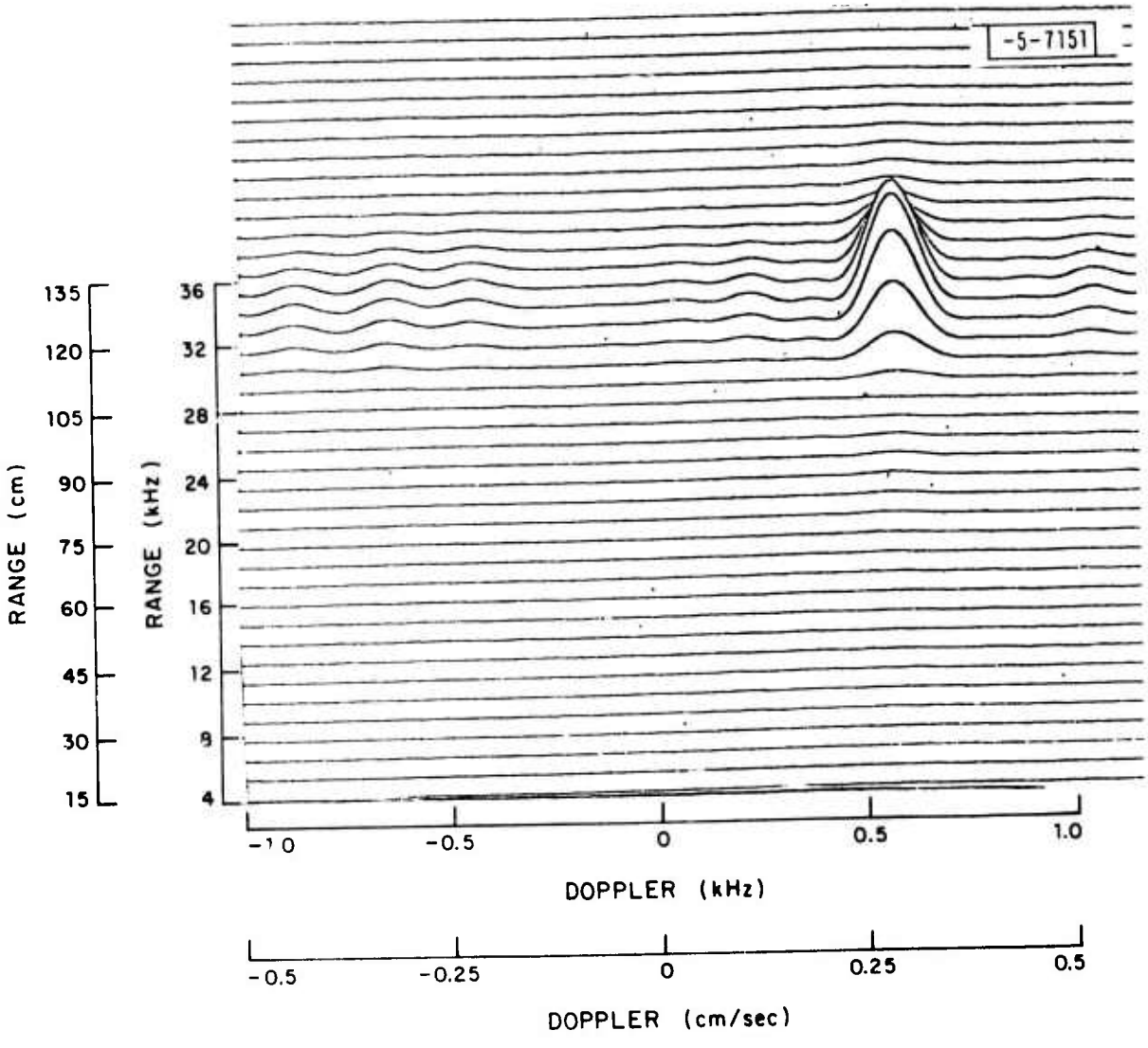

Fig. 23. 10.6 μm range-doppler image of a single moving retro.

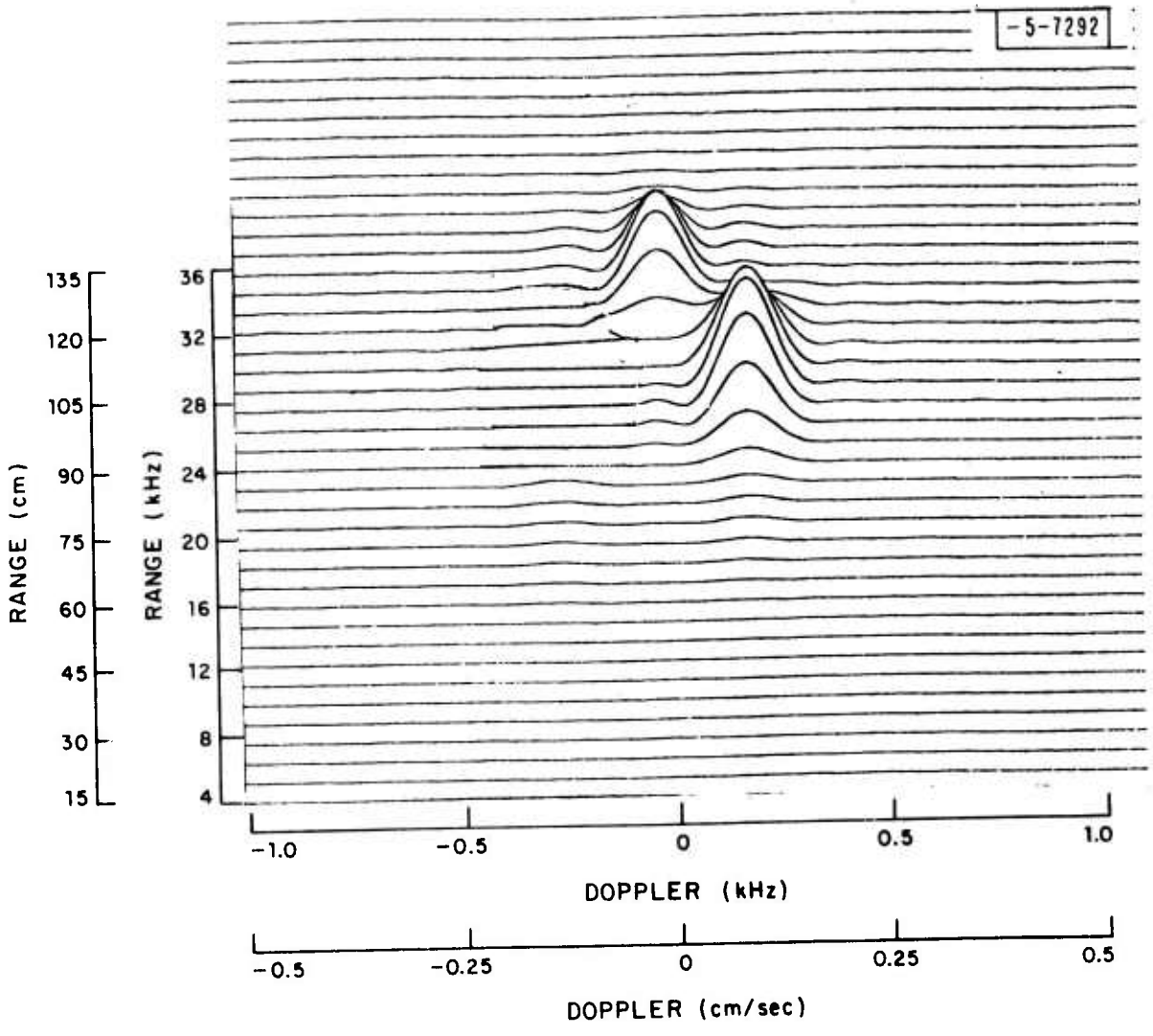

Fig. 24. 10.6 μm range-doppler image of a stationary and a moving retro.

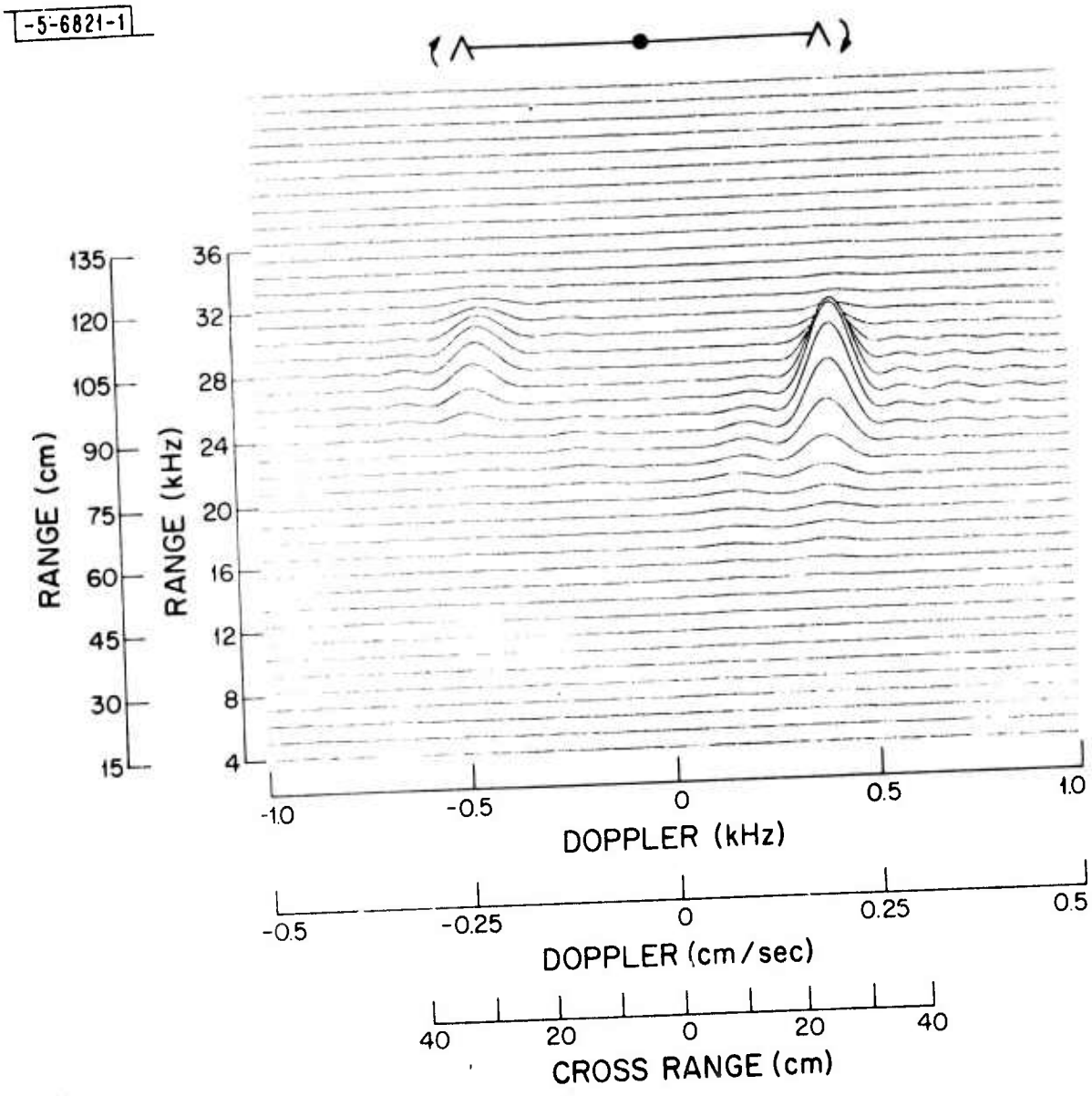

Fig. 25. 10.6 μm range-doppler image of rotating retros.

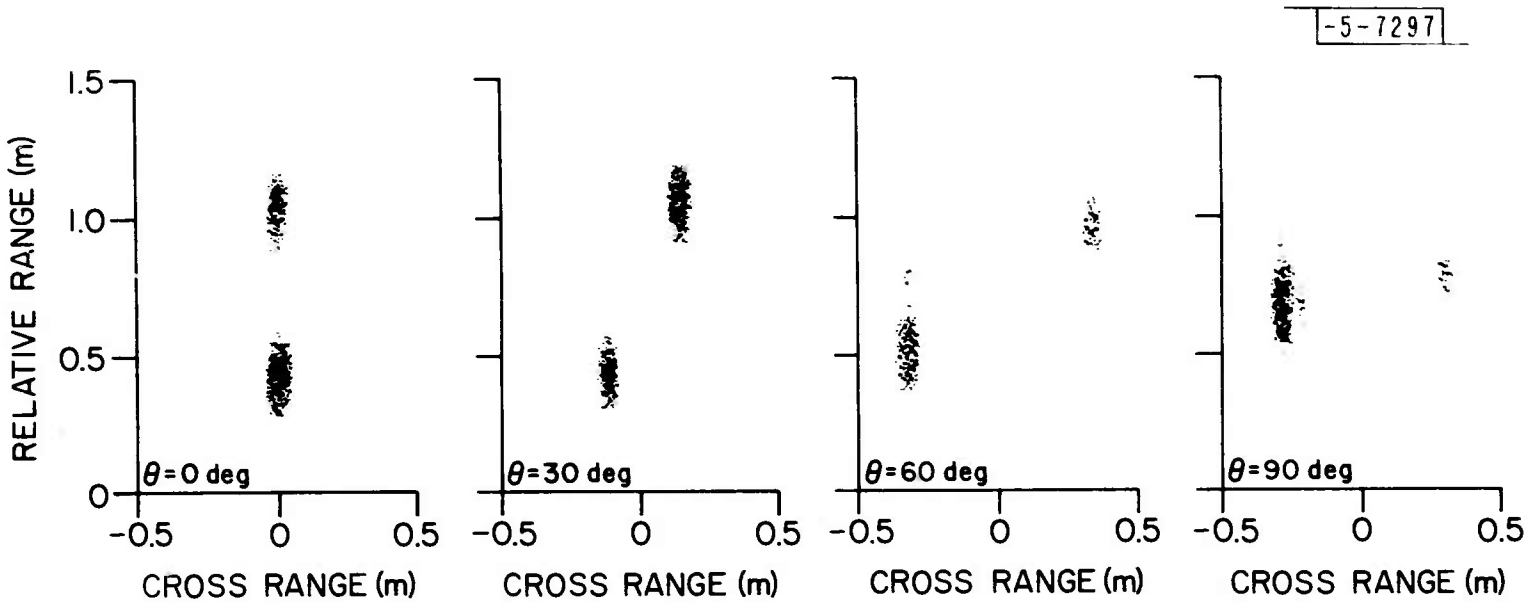

Fig. 26. 10.6 μm range-doppler images of rotating retros at different aspect angles.

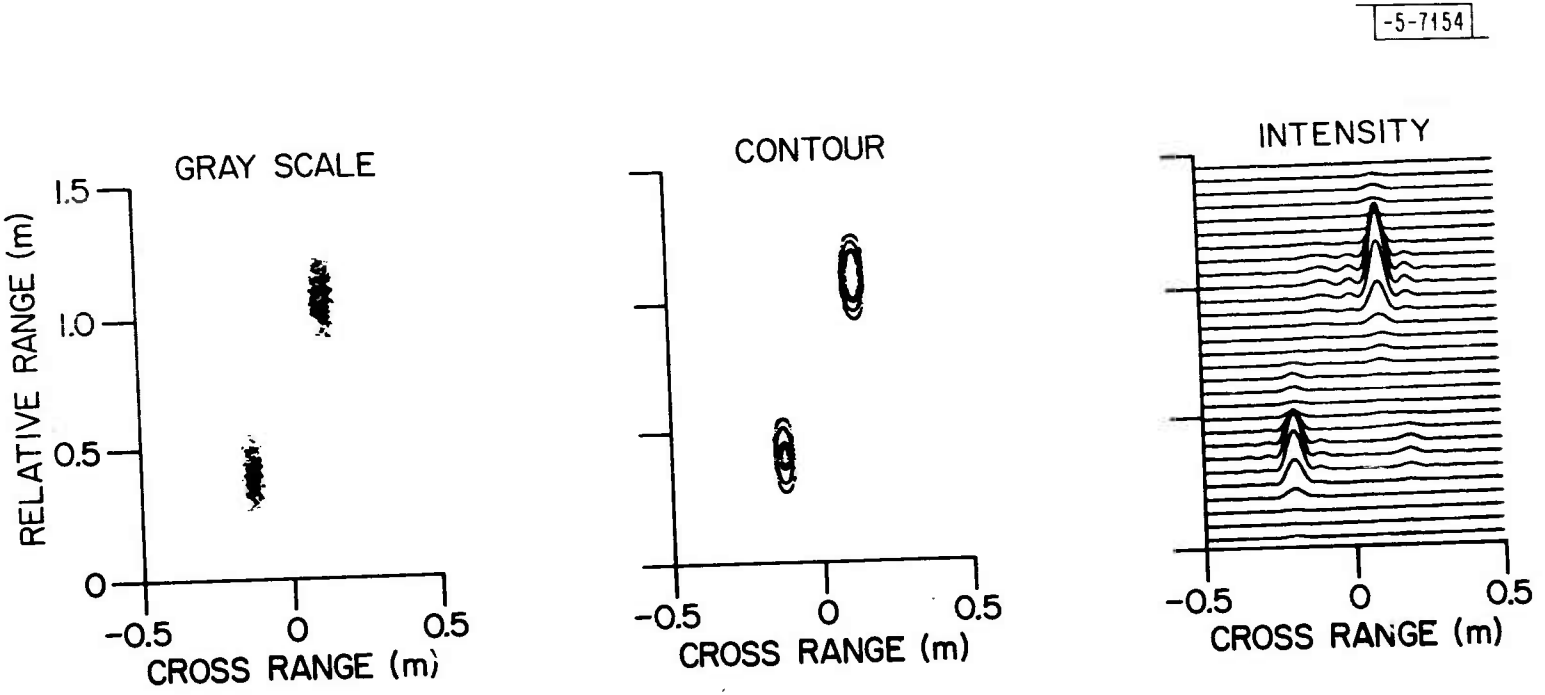

Fig. 27. 10.6 μm range-doppler image of rotating retors showing different displays.

the ambiguity function, indicating the location of the scatterers, is converted to various shades of gray levels proportional to the value of the ambiguity function. This particular image had a threshold of -10 dB, where 0 dB is the maximum value in the entire image, and any value less than -10 dB is blanked out. Similarly the second plot is a contour display with the inner-most contour representing -3 dB, the next contour representing -6 dB, and the outer one -9 dB. Thus this image has an effective dynamic range of -9 dB. In neither of these images are any sidelobes visible because the sidelobes appear at approximately -13 dB for an ideal ambiguity function representing a point scatterer (to which the retroreflectors are a good approximation). Of course various weighting techniques can be used to increase the dynamic range of the image. The last image shows an intensity display, with the sin x/x functional behavior of the ambiguity function, in the crossrange dimension, readily observed. These displays are each useful when trying to interpret specific details in any given image frame. The so called "two-dimensional image" resulting from a superposition of a sequence of images at various aspect angles would use the gray scale plots since it is the closest approximation to a photographic image.

D. System Sensitivity Enchancement by Computer Averaging

One of the advantages of post detection processing of returns is the ability to improve the signal-to-noise ratio by averaging many returns. The theoretical basis for the improvement is found in many treatises on signal processing.[4] The purpose behind this discussion is to point out

potential trouble areas in implementing signal averaging techniques in an optical system. Signal-to-noise enhancement by averaging requires a deterministic signal corrupted by random "noise." Unfortunately, in heterodyned optical signals with amplitude modulated local oscillators or electronic switching circuitry there is added to the desired deterministic signal a deterministic amplitude modulation signal which behaves, for real time observations, as an additional undesired noise component. In a microwave system this local oscillator or electronic modulation is eliminated by use of a double balanced mixer which by the use of phase alterations of the LO and signal ports can eliminate the LO amplitude modulations from the resultant mixed signal. The output contains the desired deterministic signal and random noise. The construction of double balanced optical mixer is much more difficult than the microwave device because of the wavelengths involved and is a significant research project in its own right.

The result of averaging a file consisting of signal, deterministic undesired modulation, and random noise is that the undesired deterministic modulation is enhanced as much as the signal and therefore the improvement, if any, in signal to apparent "noise" can only be as much as the difference in level between the signal and the deterministic amplitude modulated floor. In terms of real parameters this apparent noise floor is only a few dB below the random noise floor and therefore computer averaging techniques provide only marginal improvement on raw data.

We have attempted to implement the equivalent of double balanced optical mixer in the computer by sequentially recording two files of data. File 1 contains the signal, the deterministic amplitude modulation and

random noise. File 2 is recorded with the signal path block so it contains only the Local Oscillator and electronic amplitude modulation as well as random noise. File 2 is then averaged over 100 pulses to reduce the random noise by 20 dB relative to amplitude modulation spectrum. The averaged "deterministic noise" return is now subtracted from each return of File 1. The resultant processed File (File 1 - $\langle \text{File 2} \rangle_{100}$) now contains only signal and random noise and can be processed by usual coherent and non-coherent processing techniques.

Figure 28 shows a frequency and time domain return of a retro at the 60 m range. Figure 29 shows the same return with a 30 dB optical attenuator placed in the signal path. The result of coherently averaging 30 chirps of this attenuated signal is shown in Figure 30. The full 15 dB (30 times) improvement is seen demonstrating that computer averaging techniques can be used to improve signal-to-noise ratio in a chirped optical radar.

E. Dynamic Range

The ability of a system to discriminate two returns with different signal strengths is dynamic range. For the chirped radar described here the frequency domain is used to discriminate targets in range. Two targets of different cross-sections and ranges can only be detected if the side-lobes of the stronger return are below the peak of the weaker returns. The effect of computer processing in reducing sidelobes can be seen in the following simulation.

A simulated sinusoid time domain function was analyzed by the FFT subroutine and the output of the absolute-value-square of the transform

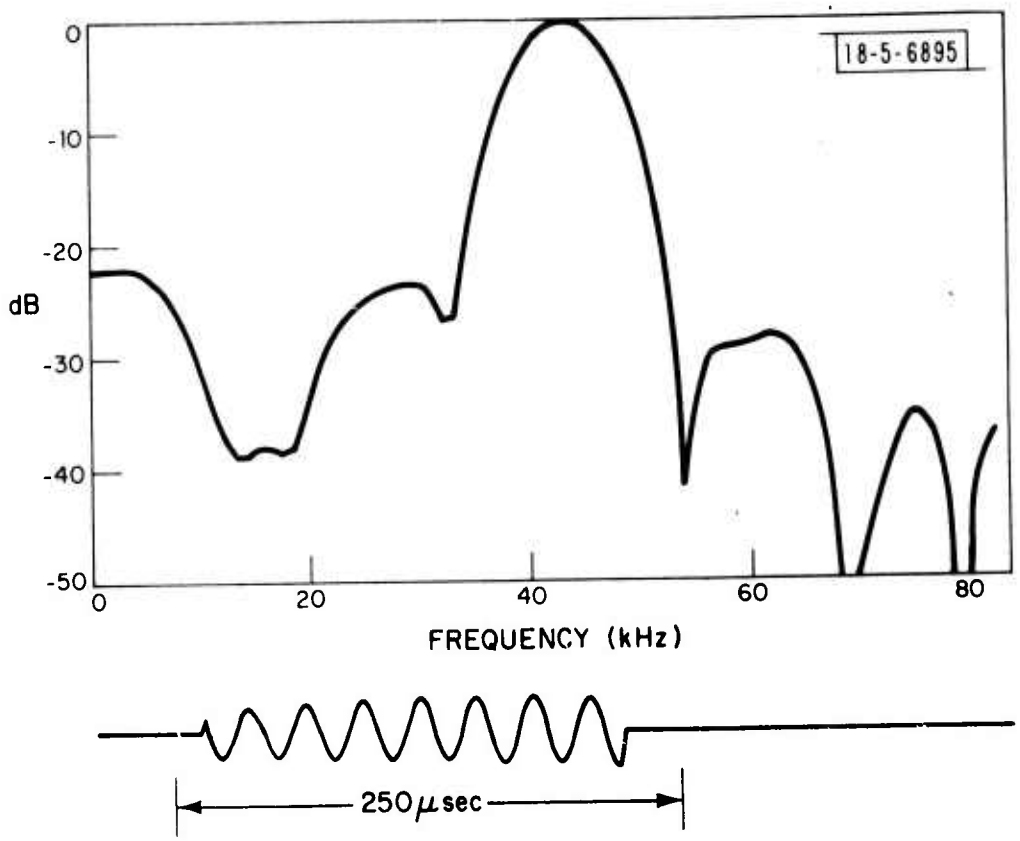

Fig. 28. Frequency spectrum and time waveform of single chirped return. 0 dB optical attenuation.

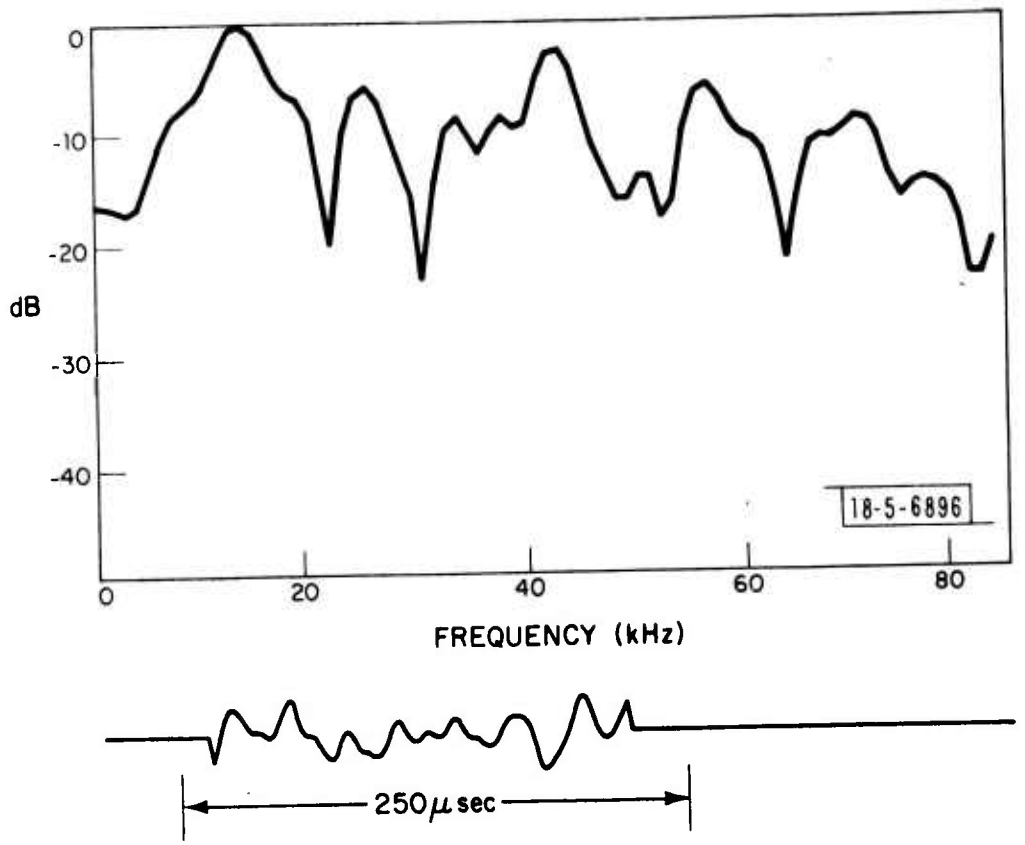

Fig. 29. Frequency spectrum and time waveform of single chirped return. 30 dB optical attenuation.

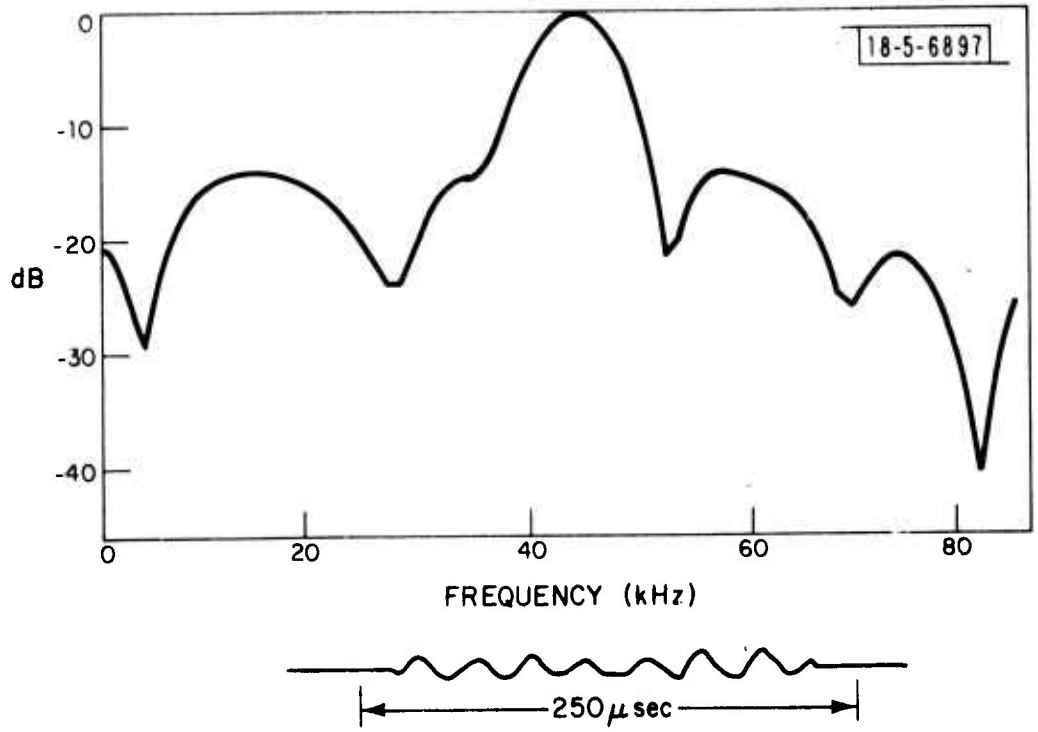

Fig. 30. Frequency spectrum and time waveform of 30 coherently average chirped returns from retroreflector with 30 dB optical attenuation.

was displayed on a logarithmic scale in Figure 8. With no Hamming weighting the output of the transform is the expected (sin x/x) function, which is the transform of a finite duration sine wave. The sidelobes corresponding to this case start at about -13 dB level. When Hamming weighting was applied, in the time domain, to the sine wave, the sidelobes of the output transform drop to below the -40 dB level. The price paid to reduce the sidelobe levels is an increased half power (3 dB) width by a factor of 1.42. It should be noted that minor deviations of the input time array from a sinusoidal functional behavior results in a lesser improvement in the sidelobe level reduction, by as much as 10 to 20 dB.

Figure 31 shows data on a 70 dB signal-to-noise ratio retroreflector that has been Hamming weighted. The dynamic range is 25 dB. Sidelobe reduction to only -25 dB rather than -40 dB can be attributed to the amplitude modulation of the input microwave signal and the non-constant amplitude response of the modulator.

VI. SUMMARY

High resolution range resolved angle scanned and range-doppler imaging have been demonstrated using a 1000 MHz linear fm chirp at 10.6 μm. Range-doppler images of a variety of targets will become available with current improvements of the modulator system and the addition of a wideband 10.6 μm amplifier.

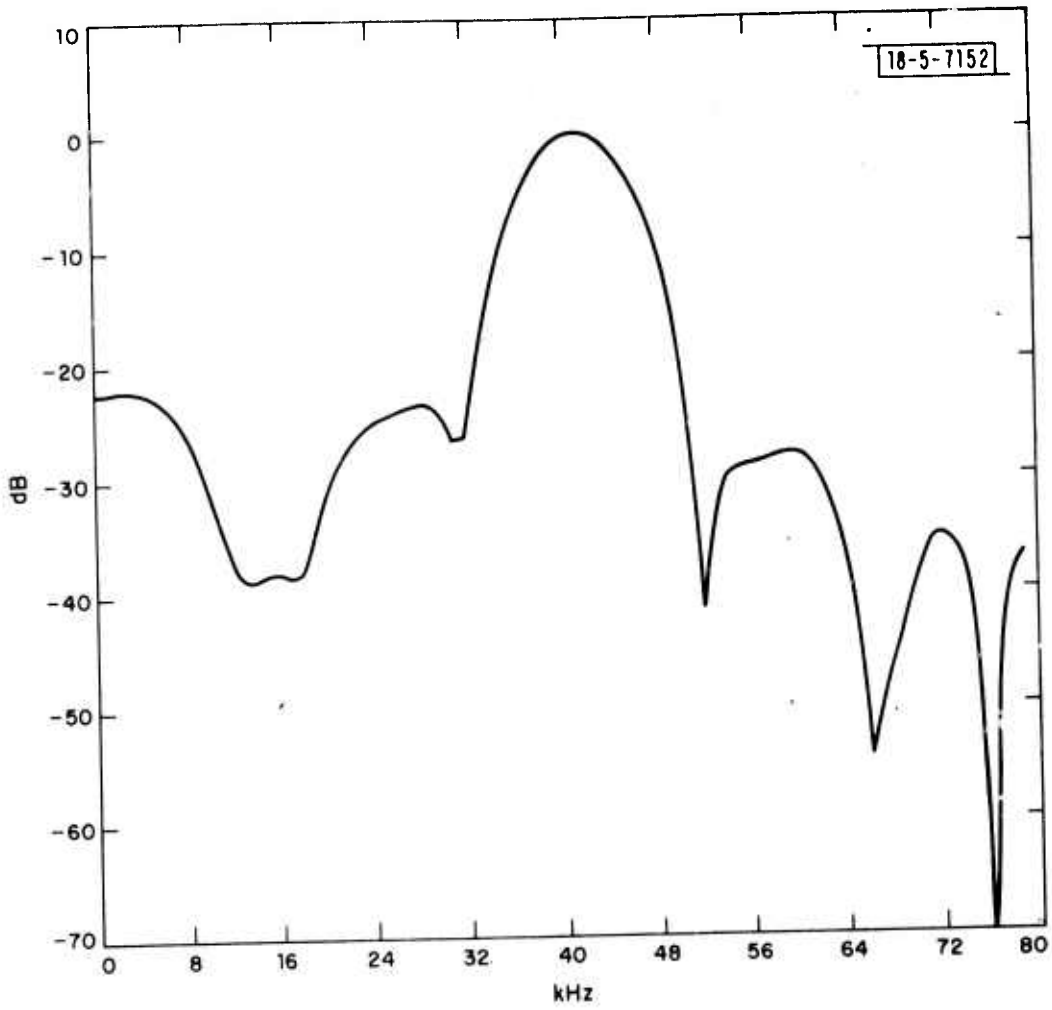

Fig. 31. 70 dB signal-to-noise ratio return that has been "Hamming" weighted.

ACKNOWLEDGMENTS

The authors wish to express their appreciation to their colleagues for their many valuable technical discussions. In particular, we wish to acknowledge W. E. Bicknell for his many contributions to the backscatter range, R. H. Kingston, L. J. Sullivan and P. A. Ingwersen for many helpful discussions, D. Bromagin for the chirp waveform generator, D. H. Bates and C. L. Summers for excellent technical assistance, R. Ponte, G. Curran and B. J. Gonsalves for data processing assistance.

REFERENCES

1. M. I. Skolnik, Introduction to Radar Systems (McGraw-Hill, New York, 1962).

2. A. E. Siegman, Proc. IEEE 54, 1350 (1966).

3. R. J. Keyes and T. M. Quist, "Low Level Coherent and Incoherent Detection in the Infrared," in Semiconductors and Semimetals, Vol. 5 (Academic Press, New York, 1970), pp. 321-359.

4. W. B. Davenport and W. L. Root, Random Signal and Noise (McGraw-Hill, New York, 1958).

UNCLASSIFIED

SECURITY CLASSIFICATION OF THIS PAGE *(When Data Entered)*

REPORT DOCUMENTATION PAGE

READ INSTRUCTIONS BEFORE COMPLETING FORM

1. REPORT NUMBER: ESD-TR-76-321	2. GOVT ACCESSION NO.
3. RECIPIENT'S CATALOG NUMBER	
4. TITLE *(and Subtitle)*: Wideband 10.6 μm Backscatter Range Interim Report	5. TYPE OF REPORT & PERIOD COVERED: Project Report
6. PERFORMING ORG. REPORT NUMBER: Project Report LRP-4	
7. AUTHOR(s): Louis R. Tomasetta, Marcus S. Edelstein, Gary M. Carter	8. CONTRACT OR GRANT NUMBER(s): F19628-76-C-0002, ARPA Order-600
9. PERFORMING ORGANIZATION NAME AND ADDRESS: Lincoln Laboratory, M.I.T., P.O. Box 73, Lexington, MA 02173	10. PROGRAM ELEMENT, PROJECT, TASK AREA & WORK UNIT NUMBERS: ARPA Order 600, Program Element No. 62301E, Project No. 6E20
11. CONTROLLING OFFICE NAME AND ADDRESS: Defense Advanced Research Projects Agency, 1400 Wilson Boulevard, Arlington, VA 22209	12. REPORT DATE: 2 November 1976
	13. NUMBER OF PAGES: 74
14. MONITORING AGENCY NAME & ADDRESS *(if different from Controlling Office)*: Electronic Systems Division, Hanscom AFB, Bedford, MA 01731	15. SECURITY CLASS. *(of this report)*: Unclassified
	15a. DECLASSIFICATION DOWNGRADING SCHEDULE

16. DISTRIBUTION STATEMENT *(of this Report)*

Approved for public release; distribution unlimited.

17. DISTRIBUTION STATEMENT *(of the abstract entered in Block 20, if different from Report)*

18. SUPPLEMENTARY NOTES

None

19. KEY WORDS *(Continue on reverse side if necessary and identify by block number)*

optical backscatter range
optical chirp radar
infrared radars
range-doppler imaging

20. ABSTRACT *(Continue on reverse side if necessary and identify by block number)*

This report summarizes the principles, hardware and performance of a high resolution 10.6 μm optical backscatter range. Included is a description of the backscatter range, optical setup and processing capabilities. Results include demonstration of the high resolution range and doppler capabilities of the wideband waveform as well as the first high resolution 10.6 μm range-resolved angle-angle scanned and range-doppler images.

DD FORM 1 JAN 73 1473 EDITION OF 1 NOV 65 IS OBSOLETE

UNCLASSIFIED

SECURITY CLASSIFICATION OF THIS PAGE *(When Data Entered)*

207 650